Electronic Supplementary Material (ESI) for Chemical Science.

Supporting Information

Robust dicopper(I) μ-boryl complexes supported by a dinucleating naphthyridine-based ligand

Pablo Ríos, Matthew S. See, Rex C. Handford, Simon J. Teat and T. D. Tilley*

Department of Chemistry, University of California, Berkeley

Advanced Light Source, Lawrence Berkeley National Laboratory

Berkeley, CA 94720-1460 (USA)

*Corresponding author: tdtilley@berkeley.edu

1. General considerations

Unless stated otherwise, all reactions were performed in a glovebox or on a Schlenk line under an atmosphere of pure N_2 using standard Schlenk techniques. Pentane, toluene, diethyl ether, tetrahydrofuran, and *ortho*-difluorobenzene (*o*-DFB) were dried and deaerated using a JC Meyers Phoenix solvent purification system. Hexamethyldisiloxane (HMDSO) was dried over potassium before being distilled. THF-d_8 was purchased from Cambridge Isotope Laboratories and dried over sodium/benzophenone before being distilled and degassed by three freeze-pump-thaw cycles. All solvents were stored over 3 Å molecular sieves for at least 24 h prior to use. $[(DPFN)Cu_2(\mu\text{-}MeCN)][NTf_2]_2$[1] and $K[B_2pin_2O^tBu]$[2] were prepared according to literature procedures. 4-(trifluoromethyl)phenylacetylene was degassed by three freeze-pump-thaw cycles and stored under nitrogen over 3 Å molecular sieves. All other reagents were purchased from commercial suppliers and used as received.

NMR spectroscopy. NMR spectra were recorded on Bruker Avance 400 and 500 MHz spectrometers and are referenced to residual protio solvent (3.58 and 1.72 ppm for THF-d_8) for ^1H NMR spectroscopy. *o*-Difluorobenzene (*o*-DFB) was used as solvent for No-deuterium (No-D) NMR experiments,[3] and was referenced to added tetramethylsilane (0.00 ppm for both ^1H and ^{13}C NMR spectroscopic experiments). ^{19}F NMR spectra were internally referenced to $CFCl_3$. ^{11}B NMR spectra were referenced to an external reference $BF_3{\cdot}OEt_2$. NMR spectra were taken at 25°C unless otherwise noted. Structural assignments were performed using HSQC and HMBC NMR spectroscopic experiments when necessary. All NMR spectra were analyzed with MestReNova.

Mass Spectrometry. Samples for ESI-MS spectrometry were prepared in THF in a nitrogen-filled glovebox. All ESI-MS spectra were obtained on a PerkinElmer AxION 2 UHPLC-TOF system equipped with an ESI source in the positive ionization mode.

Elemental analyses were performed by Dr. Elena Kreimer at the Microanalytical Facility in the College of Chemistry at the University of California, Berkeley, using a Perkin Elmer 2400 Series II combustion analyzer equipped for determination of %C, %H, and %N.

IR spectroscopy. Infrared spectra of all compounds were recorded via ATR employing an A225/Q Platinum ATR accessory with a Bruker Vertex 80 FTIR Spectrometer equipped with a room temperature DLaTGS detector using OPUS software (v. 7.2).

Cyclic Voltammetry. Electrochemical experiments were performed at 25 °C in a N_2-filled glovebox using a BASi EC Epsilon potentiostat/galvanostat and a PWR-3 Power Module. A 3 mm diameter glassy carbon electrode was used as working electrode. The electrode was polished with 0.30 µm alumina slurries, followed by additional 0.05 µm alumina slurries, rinsed with water and dried under vacuum before use. Pt wire and a $Ag/AgNO_3$ reference electrode (0.1 M $[^nBu_4N][PF_6]$ in THF as electrolyte solution) were used as counter and reference electrode, respectively. Cyclic voltammograms were recorded with software-determined iR compensation applied. Data analysis was performed with EC-Lab (v. 10.40).

2. Synthesis and characterization

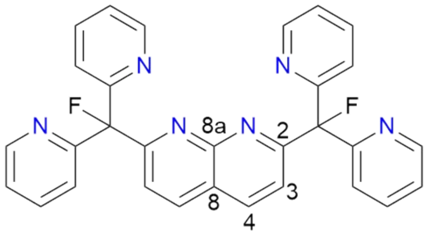

- **[(DPFN)Cu_2(μ-Bpin)][NTf_2] (2)**

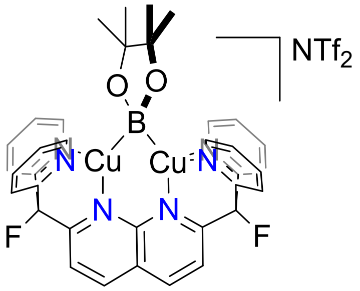

2

In a N_2-filled glovebox, a solution of **1** (40 mg, 0.032 mmol) in THF (1 mL) was added to a dram vial containing a stir bar and a suspension of KO^{t}Bu (3.7 mg, 0.033 mmol) in the same solvent (0.5 mL). The orange solution immediately became dark. The vial where the solution of **1** was prepared was rinsed with THF (0.5 mL). The rinses were added to the reaction vial, where the dark mixture was stirred at 23 °C for 30 minutes. Then, a solution of bis(pinacolato)diboron (10.5 mg, 0.041 mmol) in THF (1 mL) was added to the reaction mixture, which was left stirring at 23 °C for 15 h. The resulting dark green mixture was filtered through Celite (1 cm height in a Pasteur pipette) to a scintillation vial. The reaction vial and filter were rinsed with THF (0.5 mL). The combined filtrates were evaporated under reduced pressure, giving a green residue that was washed with pentane (2 x 1 mL) and further dried under vacuum, giving a dark green foamy solid. It was extracted with *o*DFB (2 x 1 mL) and filtered (glass microfiber in a Pasteur pipette) to a scintillation vial. The resulting dark green solution was diluted with THF (3 mL). The filtrate was layered with pentane until the 20 mL vial was full. The resulting bilayer was left to stand at 23 °C for 2 days, after which green crystals were observed. The supernatant was discarded, and pentane (20 mL) was added. The mixture was vigorously stirred for 1 hour until the crystals became a green powder. Then, the supernatant was carefully removed, and the green powder was dried under vacuum to yield 25 mg of **2** (73% yield). X-ray quality crystals were grown by extracting the product into Et_2O and layering the ether extracts with pentane. However, the solubility of the complex in this solvent is limited, giving rise to a lower yield (~20% yield).

^{1}H NMR (500 MHz, THF-d_8, 298 K): δ 9.37 (d, $^3J_{H\text{-}H}$= 4.9 Hz, 4H, 6-pyridyl C-*H*), 8.82 (d, $^3J_{H\text{-}H}$= 8.6 Hz, 2H, 4-naph C-*H*), 8.39 (dd, $^3J_{H\text{-}H}$= 8.6 Hz, $^4J_{H\text{-}F}$= 3.0 Hz, 2H, 3-naph C-*H*), 8.14 (dd, $^3J_{H\text{-}H}$= 8.1 Hz, $^4J_{H\text{-}H}$= 3.2 Hz, 4H, 3-pyridyl C-*H*), 8.03 (td, $^3J_{H\text{-}H}$= 8.0 Hz, $^4J_{H\text{-}H}$= 1.5 Hz, 4H, 4-pyridyl C-*H*), 7.51 (dd, $^3J_{H\text{-}H}$= 7.4 Hz, $^3J_{H\text{-}H}$= 5.3 Hz, 4H, 5-pyridyl C-*H*) 1.36 (s, 12 H, C*H*$_3$C) ppm. **^{11}B{^{1}H} NMR (160 MHz, THF-*d*$_8$, 298 K): δ** 44.8 (bs, Bpin) ppm. **^{13}C{^{1}H} NMR (125 MHz, THF-*d*$_8$, 298 K): δ** 160.30 (d, $^2J_{C-F}$= 30.9 Hz, 2-naph *C*$_q$), 154.06 (d, $^2J_{C-F}$= 29.0 Hz, 2-pyridyl *C*$_q$), 152.03 (d, $^4J_{C-F}$= 2.8 Hz, 6-pyridyl *C*-H), 151.42 (8a-naph *C*$_q$), 141.96 (d, $^4J_{C-F}$= 3 Hz, 4-naph *C*-H), 139.90 (d, $^4J_{C-F}$= 3.1 Hz, 4-pyridyl *C*-H), 125.30 (5-pyridyl *C*-H), 123.74 (8-naph *C*$_q$), 121.21 (d, $^3J_{C-F}$= 13.7 Hz, 3-pyridyl *C*-H), 120.18 (d, $^3J_{C-F}$= 13.4 Hz, 3-naph *C*-H), 95.13 (d, $^1J_{C-F}$= 187.4 Hz, *C*-F), 80.96 (CH$_3$*C*), 26.50 (*C*H$_3$C) ppm. **^{19}F{^{1}H} NMR (470 MHz, THF-*d*$_8$, 298 K): δ** -79.82 (s, -SO$_2$CF$_3$), -177.47 (s, DPFN) ppm.

Anal. Calcd for: $C_{38}H_{32}BCu_2F_8N_7O_6S_2$: C, 44.02; H, 3.11; N, 9.46. Found: C, 44.14; H, 3.31; N, 9.34.

HRMS(ESI) Calculated for $[C_{36}H_{32}BCu_2F_2N_6O_2]^+$: 755.1235. Found: 755.1224.

- **[(DPFN)Cu$_2$(*μ*-O^{t}Bu)][NTf$_2$] (3)**

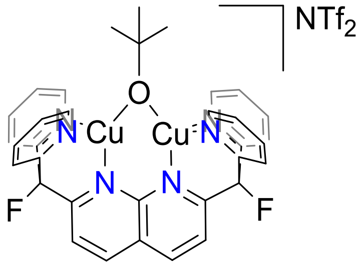

3

In a N$_2$-filled glovebox, a solution of **1** (40 mg, 0.032 mmol) in THF (1 mL) was added to a dram vial containing a stir bar and a suspension of KO^{t}Bu (3.7 mg, 0.033 mmol) in the same solvent (0.5 mL). The orange solution immediately became dark. The original vial containing the solution of **1** was rinsed with THF (0.5 mL) and the combined rinses were added to the reaction vial, after which the dark mixture was stirred at 23 °C for 30 minutes. Then, the resulting dark mixture was filtered through Celite (1 cm height in a Pasteur pipette) into a scintillation vial. The reaction vial and filter were rinsed with THF (0.5 mL). Pentane (15-16 mL) was added to the combined filtrates with vigorous stirring, giving a yellowish supernatant and a dark solid. It was left to stand at -35 °C for 30 minutes, after which the supernatant was carefully removed. The solid was extracted with *o*DFB (1 mL) and the extract was filtered through Celite. The resulting solution was analyzed by NMR:

^{1}H NMR (500 MHz, *o*-DFB, 298 K): δ 8.99 (d, $^3J_{H-H}$= 5.0 Hz, 4H, 6-pyridyl C-*H*), 8.25 (d, $^3J_{H-H}$= 8.6 Hz, 2H, 4-naph C-*H*), 8.12 (dd, $^3J_{H-H}$= 8.6 Hz, $^4J_{H-F}$= 3.2 Hz, 2H, 3-naph C-*H*), 7.91 (dd, $^3J_{H-H}$= 8.1 Hz, $^4J_{H-H}$= 3.0 Hz, 4H, 3-pyridyl C-*H*), 7.73 (td, $^3J_{H-H}$= 7.9 Hz, $^4J_{H-H}$= 1.7 Hz, 4H, 4-pyridyl C-*H*), 7.25 (ddd, $^3J_{H-H}$= 7.6 Hz, $^3J_{H-H}$= 5.0 Hz, $^4J_{H-H}$= 1.1 Hz, 4H, 5-pyridyl C-*H*), 1.76 (s, 9 H, (C*H*$_3$)$_3$C) ppm. **^{13}C{^{1}H} NMR (125 MHz, *o*-DFB, 298 K): δ** 160.65 (d, $^2J_{C-F}$= 29.7 Hz, 2-naph *C*$_q$), 154.78 (d, $^2J_{C-F}$= 29.8 Hz, 2-pyridyl *C*$_q$), 151.30 (8a-naph *C*$_q$), 149.80 (d, $^4J_{C-F}$= 2.7 Hz, 6-pyridyl *C*-H), 139.66 (d, $^4J_{C-F}$= 3.6 Hz, 4-naph *C*-H), 138.49 (d, $^4J_{C-F}$= 3.2 Hz, 4-pyridyl *C*-H), 124.82 (5-pyridyl *C*-H), 123.06 (8-naph *C*$_q$), 120.91 (d, $^3J_{C-F}$= 14.7 Hz, 3-

pyridyl *C*-H), 119.82 (d, $^3J_{C-F}$= 17.5 Hz, 3-naph *C*-H), 93,91 (d, $^1J_{C-F}$ = 184.6 Hz, *C*-F), 71.03 ($(CH_3)_3C$), 36.31 ($(CH_3)_3C$) ppm. **^{19}F{^{1}H} NMR (470 MHz, *o*-DFB, 298 K): δ** -79.01 (s, -SO_2CF_3), -168.76 (s, DPFN) ppm.

The formation of an insoluble material after exposing complex **3** to vacuum prevented the synthesis of analytically pure solid samples of this compound.

- **[(DPFN)Cu$_2$(*μ*-Bcat)][NTf$_2$] (4)**

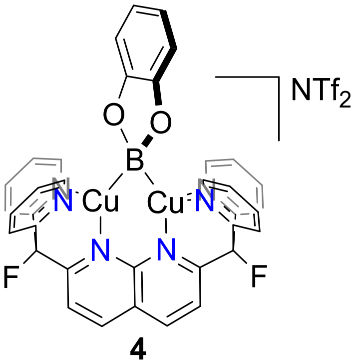

4

In a N_2-filled glovebox, a solution of **1** (70 mg, 0.057 mmol) in THF (1 mL) was added to a dram vial containing a stir bar and a suspension of KO*^t*Bu (6.7 mg, 0.06 mmol) in the same solvent (0.5 mL). The orange solution immediately became dark. The vial where the solution of **1** was prepared was rinsed with THF (1 mL), and the rinses were added to the reaction vial, where the dark mixture was stirred at 23 °C for 30 minutes. Then, a solution of bis(catecholato)diboron (17.6 mg, 0.074 mmol) in THF (1 mL) was added to the reaction mixture, which was left stirring at 23 °C for 2 h. The resulting dark purple mixture was then filtered through Celite (1 cm height in a Pasteur pipette) to a scintillation vial. The reaction vial and filter were rinsed with THF (1 mL). The combined filtrates were evaporated under reduced pressure, giving a residue that was washed with toluene (1 mL) and pentane (2 x 1 mL) and further dried under vacuum, giving a greenish-grey solid. This was extracted with *o*DFB (1 mL + 2 x 0.5 mL) and filtered (glass microfiber in a Pasteur pipette) into a scintillation vial. The resulting dark purple solution was diluted with THF (3 mL). The filtrate was layered with pentane until the 20 mL vial was full. The resulting bilayer was left to stand at 23 °C for 2 days, after which green crystals were observed. The supernatant was discarded, and pentane (20 mL) was added. The resulting mixture was vigorously stirred for 1 hour until the crystals became a dark green powder. Then, the supernatant was carefully removed, and the dark green powder was dried under vacuum to yield 46.1 mg of **4** (79% yield).

^{1}H NMR (500 MHz, THF-*d*$_8$, 298 K): δ 9.30 (d, $^3J_{H-H}$= 4.7 Hz, 4H, 6-pyridyl C-*H*), 8.85 (d, $^3J_{H-H}$= 8.6 Hz, 2H, 4-naph C-*H*), 8.45 (dd, $^3J_{H-H}$= 8.6 Hz, $^4J_{H-F}$= 2.9 Hz, 2H, 3-naph C-*H*), 8.16 (dd, $^3J_{H-H}$= 8.2 Hz, $^4J_{H-H}$= 2.7 Hz, 4H, 3-pyridyl C-*H*), 8.04 (td, $^3J_{H-H}$= 7.9 Hz, $^4J_{H-H}$= 0.9 Hz, 4H, 4-pyridyl C-*H*), 7.54 (m, 4H, 5-pyridyl C-*H*), 7.30 (dd, $^3J_{H-H}$= 5.5 Hz, $^4J_{H-H}$= 3.5 Hz, 2H, Bcat C-H_{arom}), 6.96 (dd, $^3J_{H-H}$= 5.5 Hz, $^4J_{H-H}$= 3.4 Hz, 2H, Bcat C-H_{arom}), ppm. **^{11}B{^{1}H} NMR (160 MHz, THF-*d*$_8$, 298 K): δ** 47.7 (bs, Bcat) ppm. **^{13}C{^{1}H} NMR (125 MHz, THF-*d*$_8$, 298 K): δ** 160.32 (d, $^2J_{C-F}$= 30.8 Hz, 2-naph C_q), 153.90 (d, $^2J_{C-F}$= 28.9 Hz, 2-pyridyl C_q), 152.01 (d, $^4J_{C-F}$= 2.9 Hz, 6-pyridyl *C*-H), 151.39 (8a-naph C_q), 151.39 (Bcat, *C*-O),* 142.71 (d, $^4J_{C-F}$=

2.8 Hz, 4-naph *C*-H), 140.25 (d, $^4J_{C\text{-}F}$= 3.4 Hz, 4-pyridyl *C*-H), 125.64 (5-pyridyl *C*-H), 123.89 (8-naph C_q), 121.61 (Bcat *C*-H$_{arom}$), 121.32 (d, $^3J_{C\text{-}F}$= 14.0 Hz, 3-pyridyl *C*-H), 120.37 (d, $^3J_{C\text{-}F}$= 13.4 Hz, 3-naph *C*-H), 111.86 (Bcat *C*-H$_{arom}$), 95.0 (d, $^1J_{C\text{-}F}$= 187.9 Hz, *C*-F) ppm. **^{19}F{^{1}H} NMR (470 MHz, THF-*d*$_8$, 298 K): δ** -79.85 (s, -SO_2CF_3), -177.05 (s, DPFN) ppm. * Assignments done based on HMBC cross-peaks.

Anal. Calcd for: $C_{38}H_{24}BCu_2F_8N_7O_6S_2$: C, 44.37; H, 2.35; N, 9.53. Found: C, 43.88; H, 2.38; N, 9.25.

HRMS(ESI) Calculated for $[C_{36}H_{24}BCu_2F_2N_6O_2]^+$: 747.0609. Found: 747.0628.

- **Reactivity of 2 and 4 with terminal phenylacetylenes**

In a N_2-filled glovebox, phenylacetylene or 4-(trifluoromethyl)phenylacetylene (1.5 equiv for complex **2**, 6 equiv for complex **4**) was added by means of a microsyringe to a solution of dicopper boryl complex (0.009 mmol) in 0.6 mL of solvent (THF for complex **2** or *o*-DFB for complex **4**). The resulting solution was transferred to a J. Young NMR tube, after which it was placed in an oil bath (70 °C for complex **2**, 100 °C for complex **4**). The reaction was monitored by ^{1}H NMR.

- **Reactivity of between 5 and B_2cat_2**

Figure S21 and S21A exhibit the formation of complex **4** upon reaction between **5** and B_2cat_2. Attempts to characterize the byproduct of this reaction involved filtration of the reaction mixture through silica followed by solvent evaporation, which produced a colorless solid that is soluble in C_6D_6. Whereas NMR analysis suggests the presence of a single species [(^{1}H NMR (500 MHz, C_6D_6, 298 K): δ 7.07, 6.81, 6.64, 6.55 (dd, J = 5.9 Hz, 3.5 Hz, 1H each) ppm; ^{11}B{^{1}H} NMR (160 MHz, C_6D_6, 298 K): δ 31.1 (bs) ppm; ^{19}F{^{1}H} NMR (470 MHz, C_6D_6, 298 K): δ -62.4 (s) ppm], additional experimental evidence would be necessary to confidently determine the structure of this compound, given that (for example) mass spectrometry experiments provided no conclusive results.

3. NMR spectra

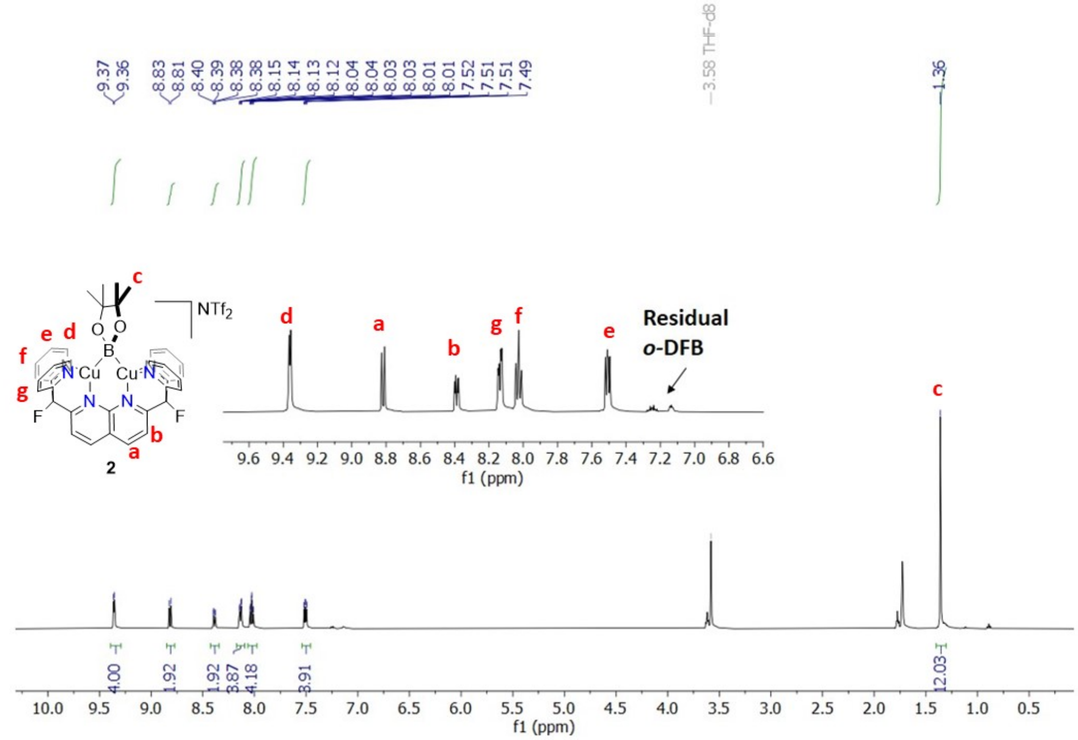

Figure S1. ^{1}H NMR (THF-d_8, 500 MHz) of complex **2**.

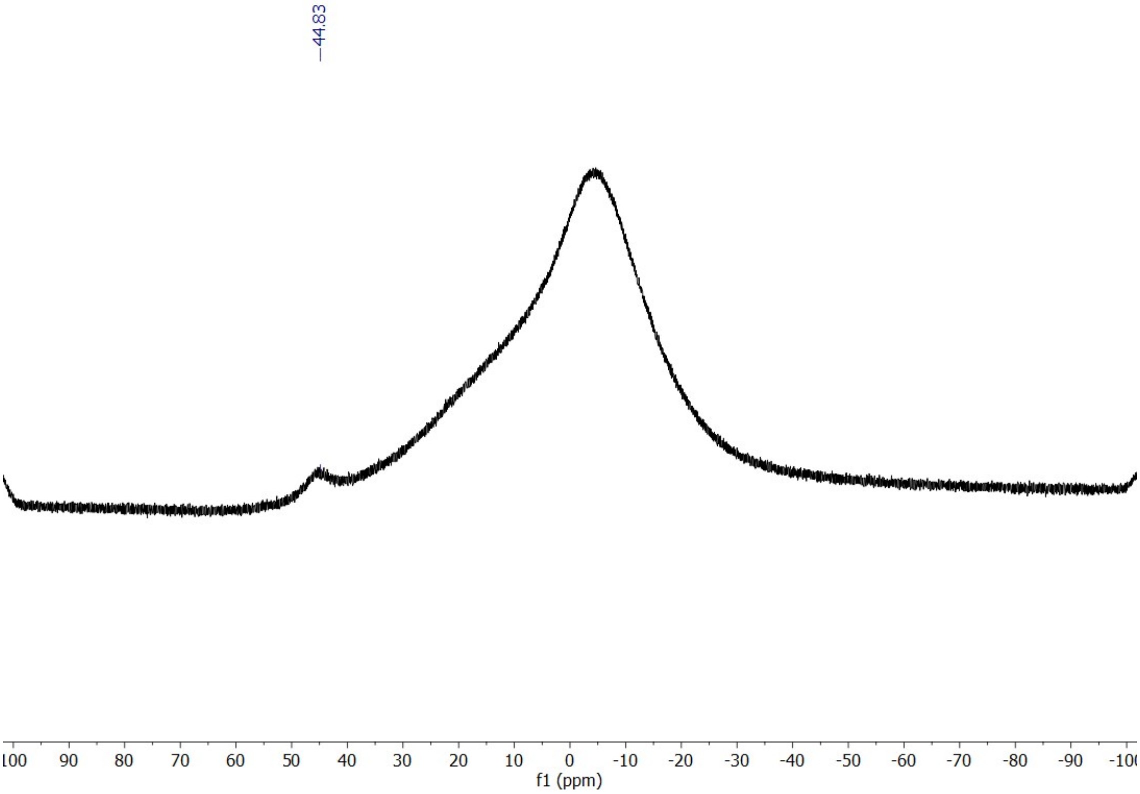

Figure S2. ^{11}B NMR (THF-d_8, 160 MHz) of complex **2**.

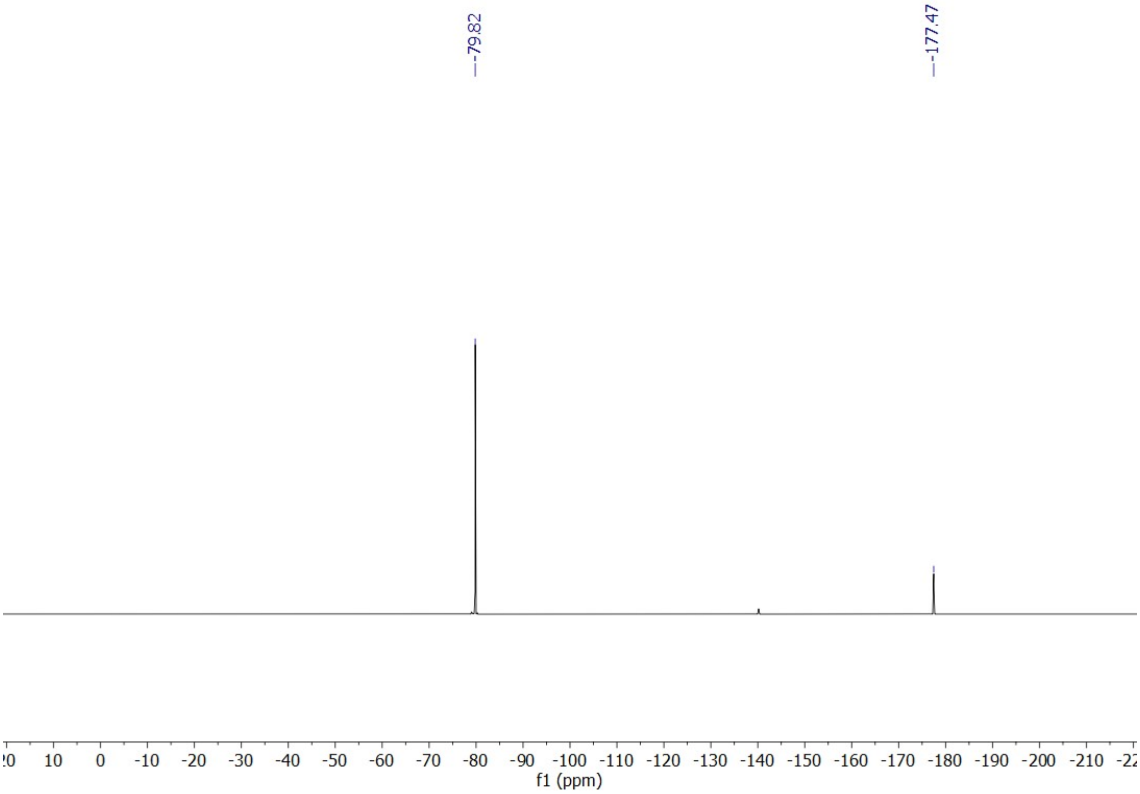

Figure S3. ^{19}F NMR (THF-d_8, 470 MHz) of complex **2**.

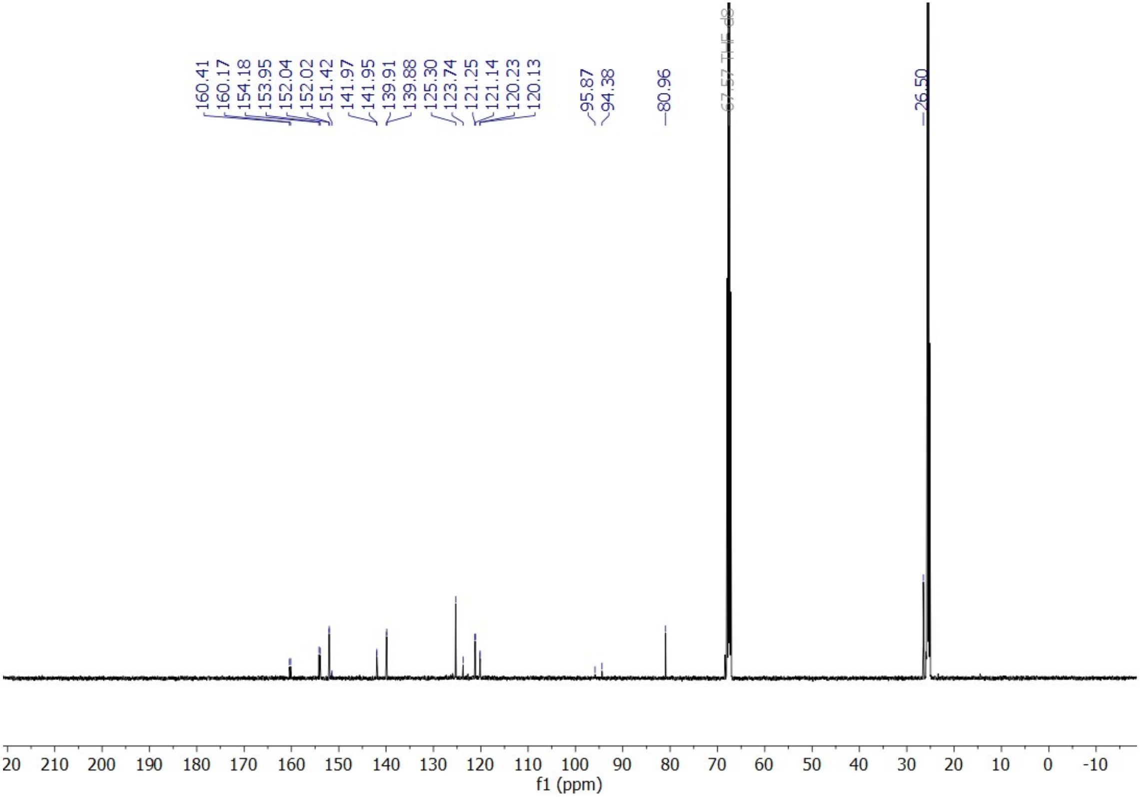

Figure S4. ^{13}C NMR (THF-d_8, 125 MHz) of complex **2**.

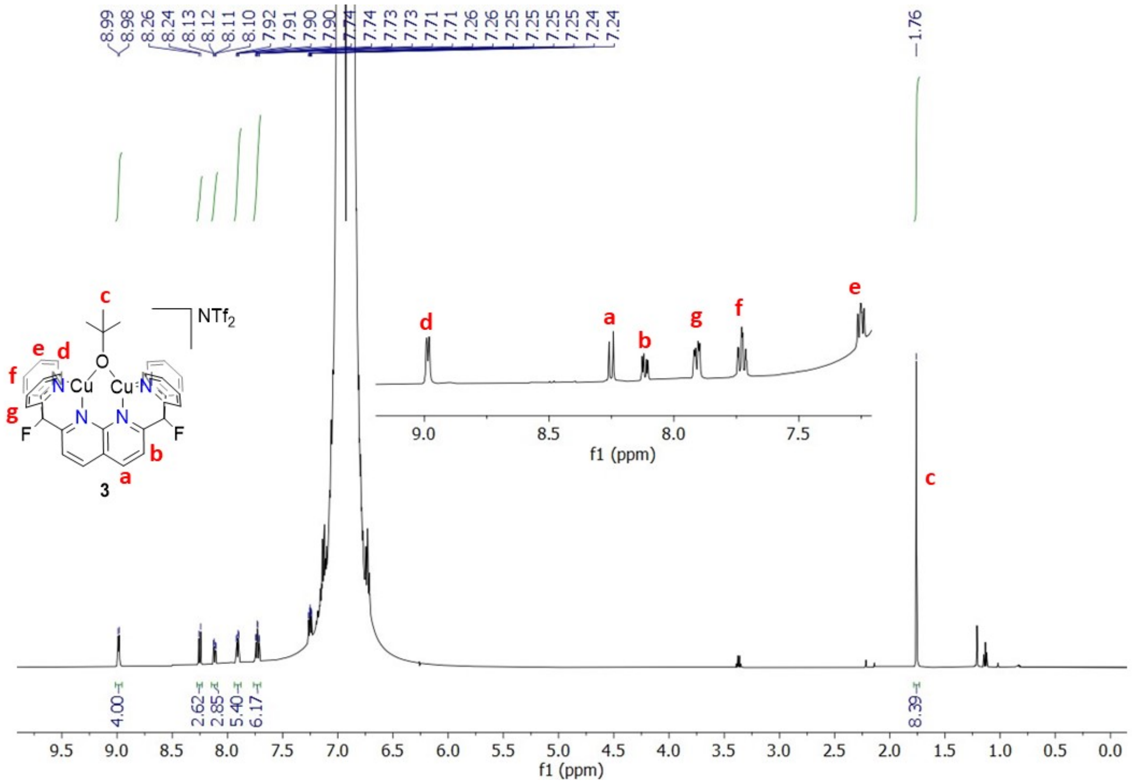

Figure S5. ^{1}H NMR (*o*-DFB, 500 MHz) of complex **3**.

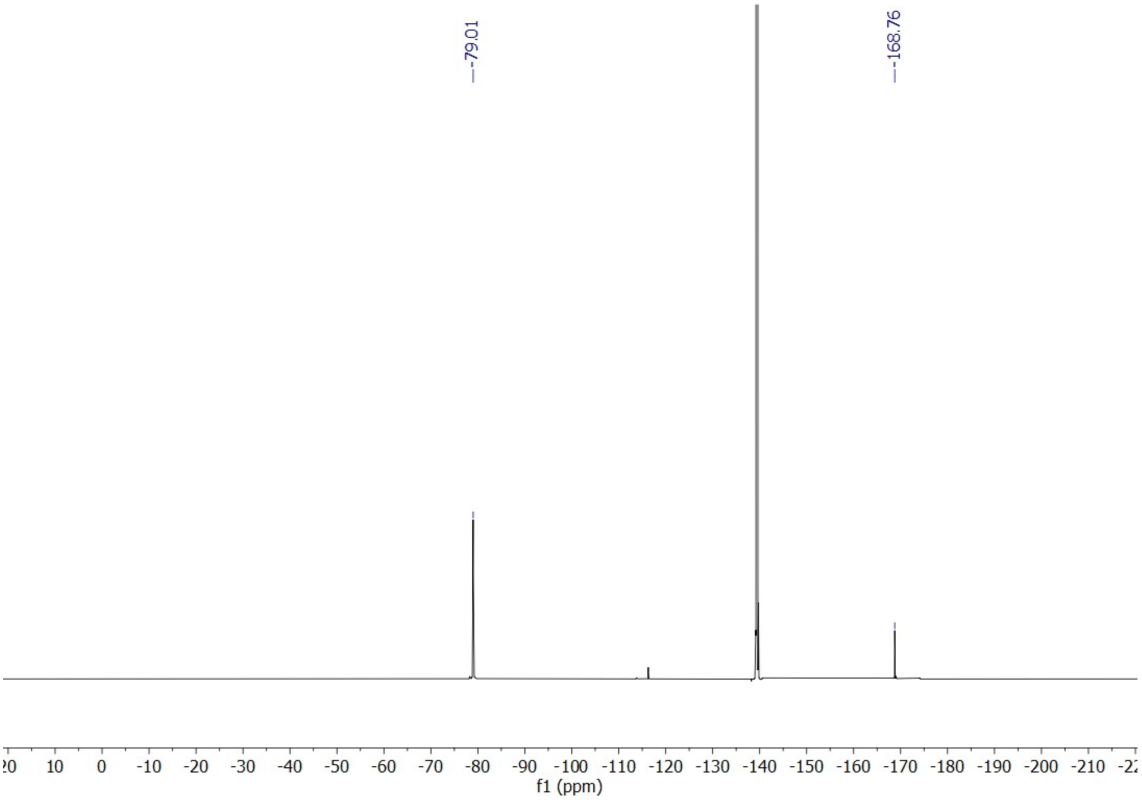

Figure S6. ^{19}F NMR (*o*-DFB, 470 MHz) of complex **3**.

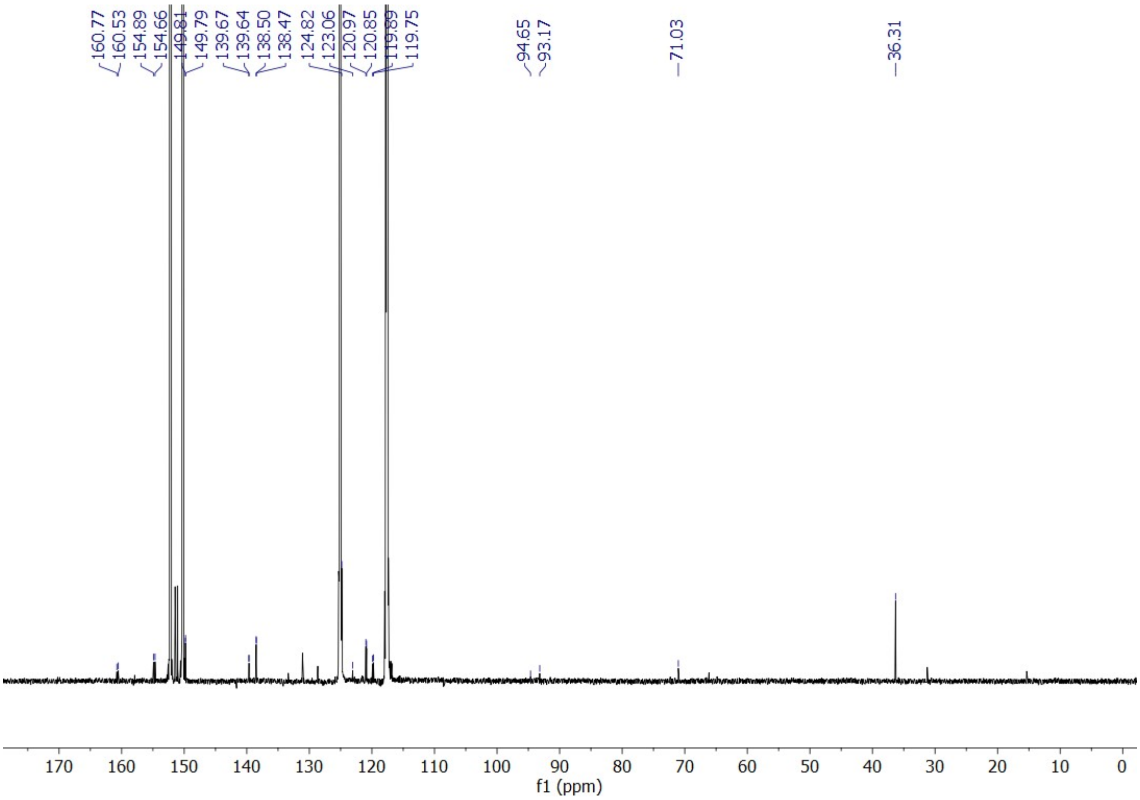

Figure S7. ^{13}C NMR (*o*-DFB, 125 MHz) of complex **3**.

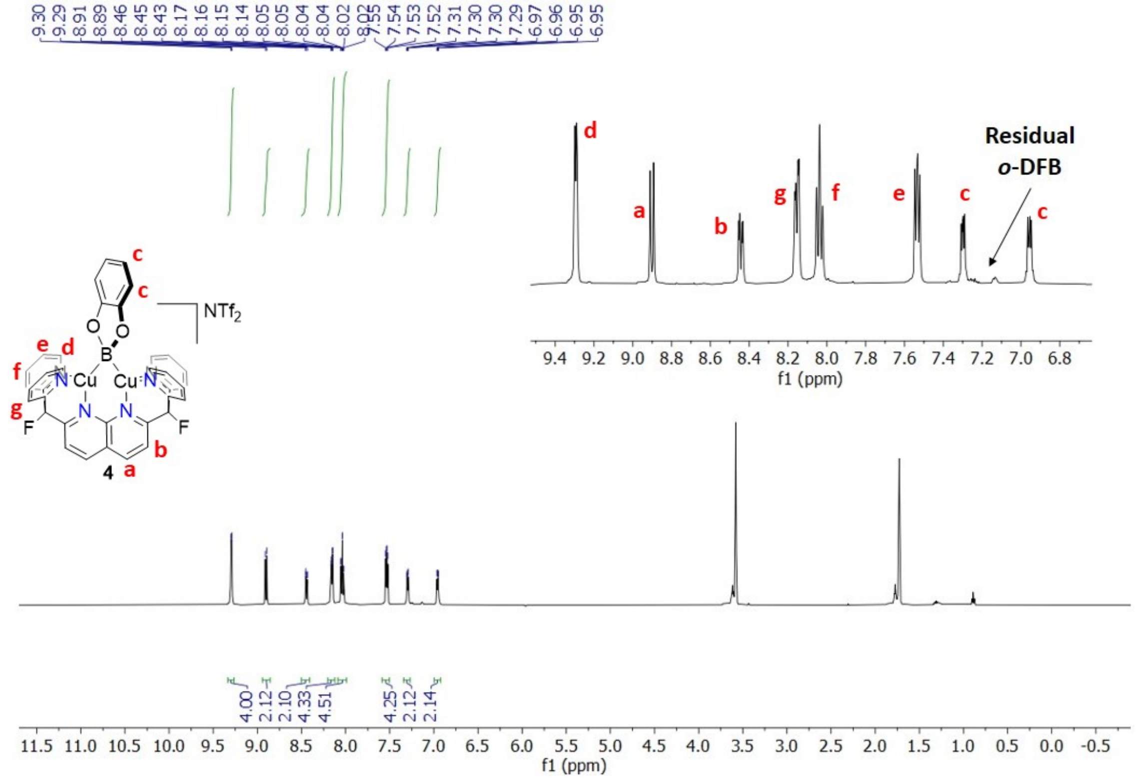

Figure S8. ^{1}H NMR (THF-d_8, 500 MHz) of complex **4**.

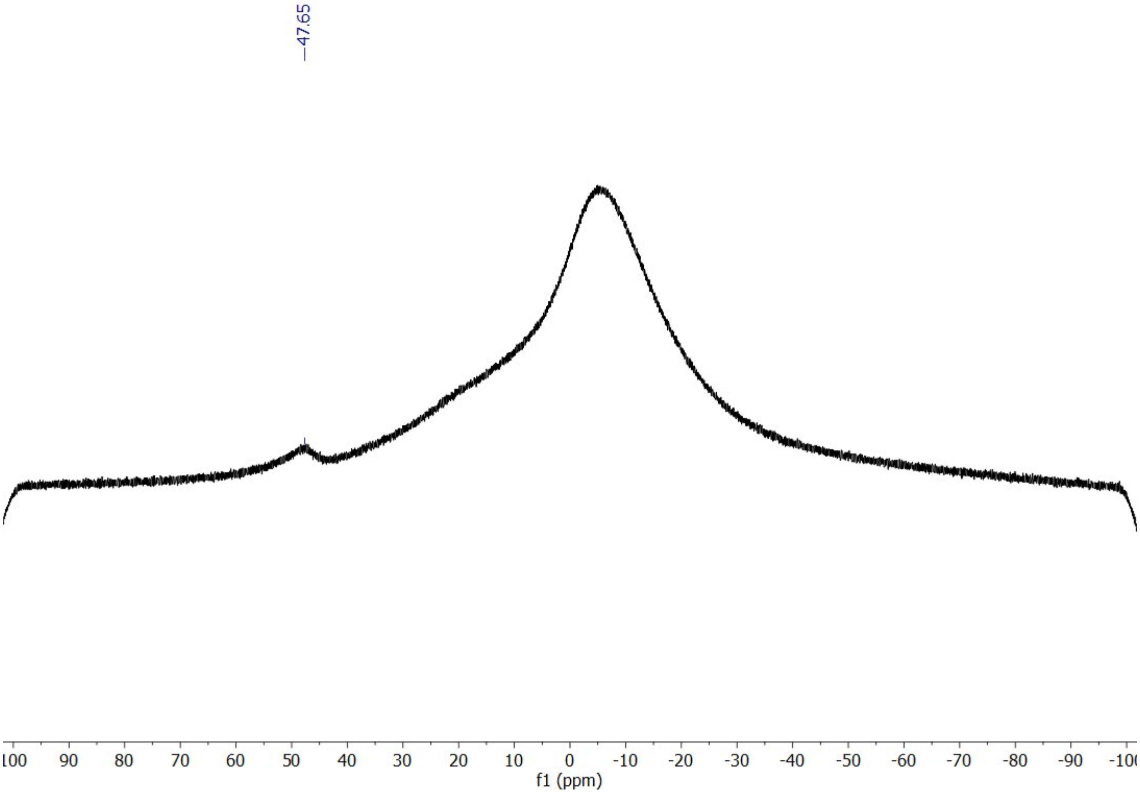

Figure S9. ^{11}B NMR (THF-d_8, 160 MHz) of complex **4**.

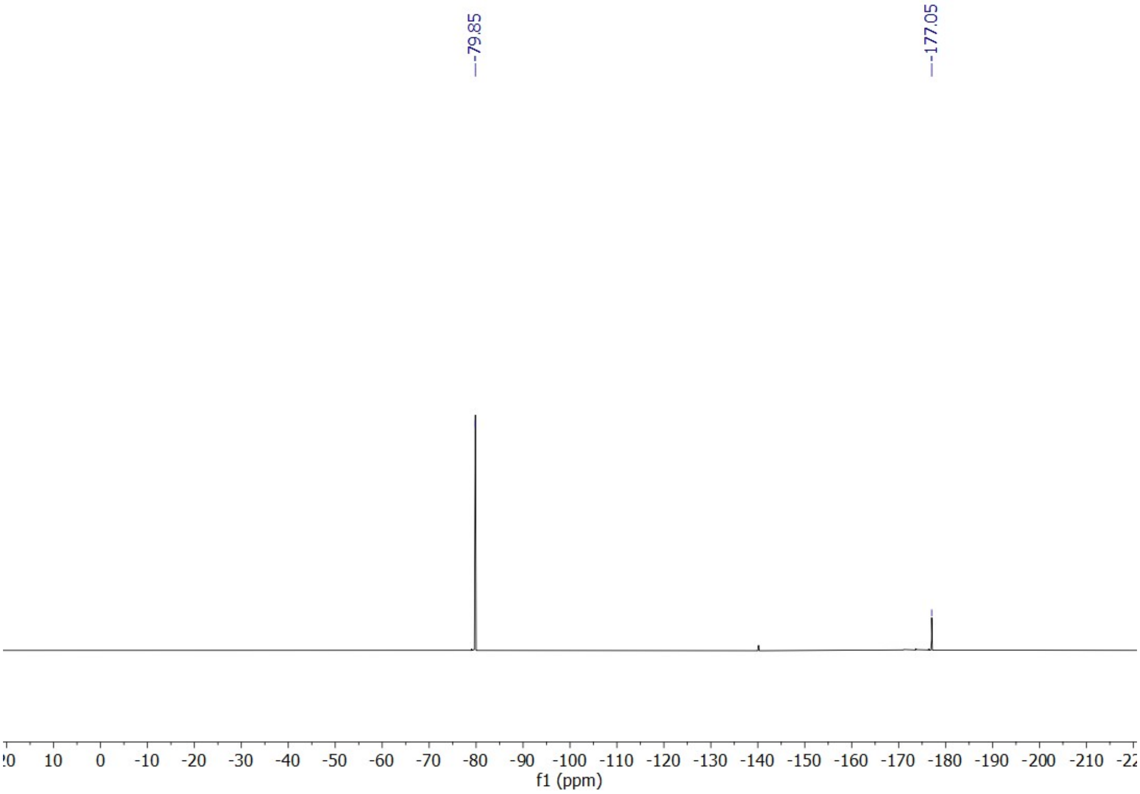

Figure S10. ^{19}F NMR (THF-d_8, 470 MHz) of complex **4**.

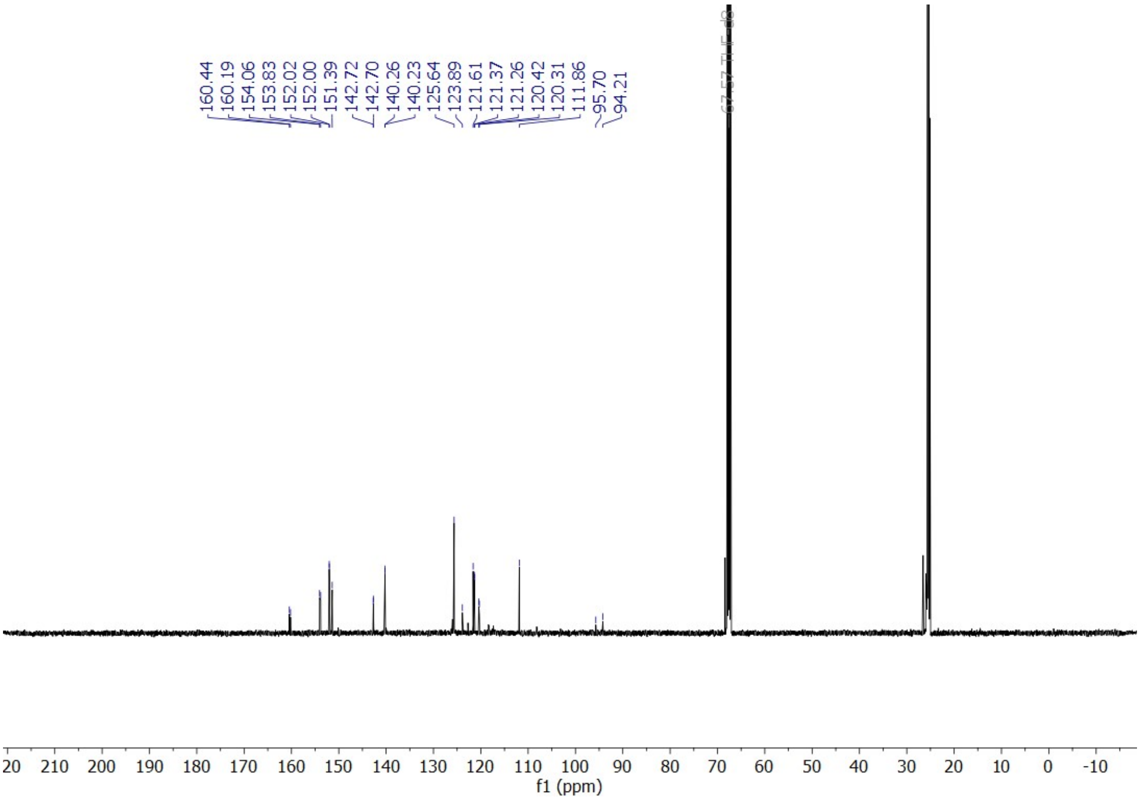

Figure S11. ^{13}C NMR (THF-d_8, 125 MHz) of complex **4**.

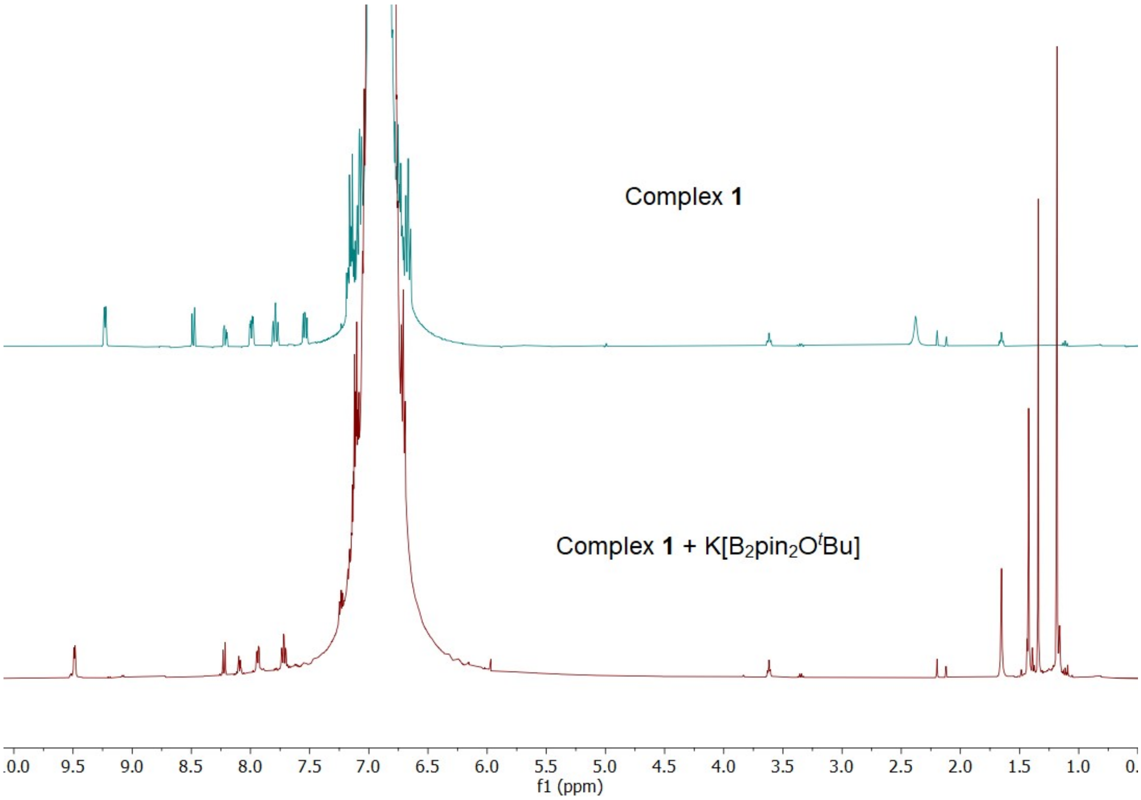

Figure S12. Comparison of the ^{1}H NMR spectra (*o*-DFB, 500 MHz) of complex **1** (top) and **1** + K[$B_2pin_2O^tBu$] on a 15 mg scale (bottom)

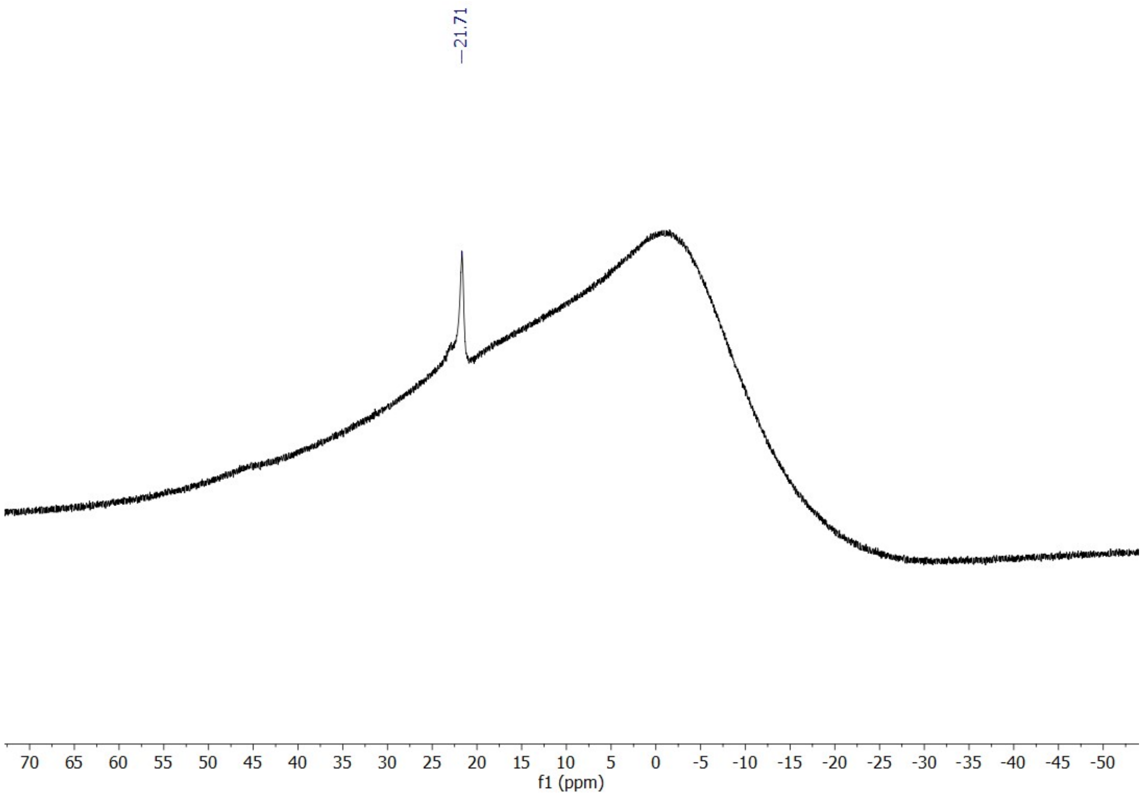

Figure S13. ^{11}B NMR spectrum (*o*-DFB, 160 MHz) of complex **1** + K[$B_2pin_2O^tBu$], revealing the presence of ^{t}BuOBpin.

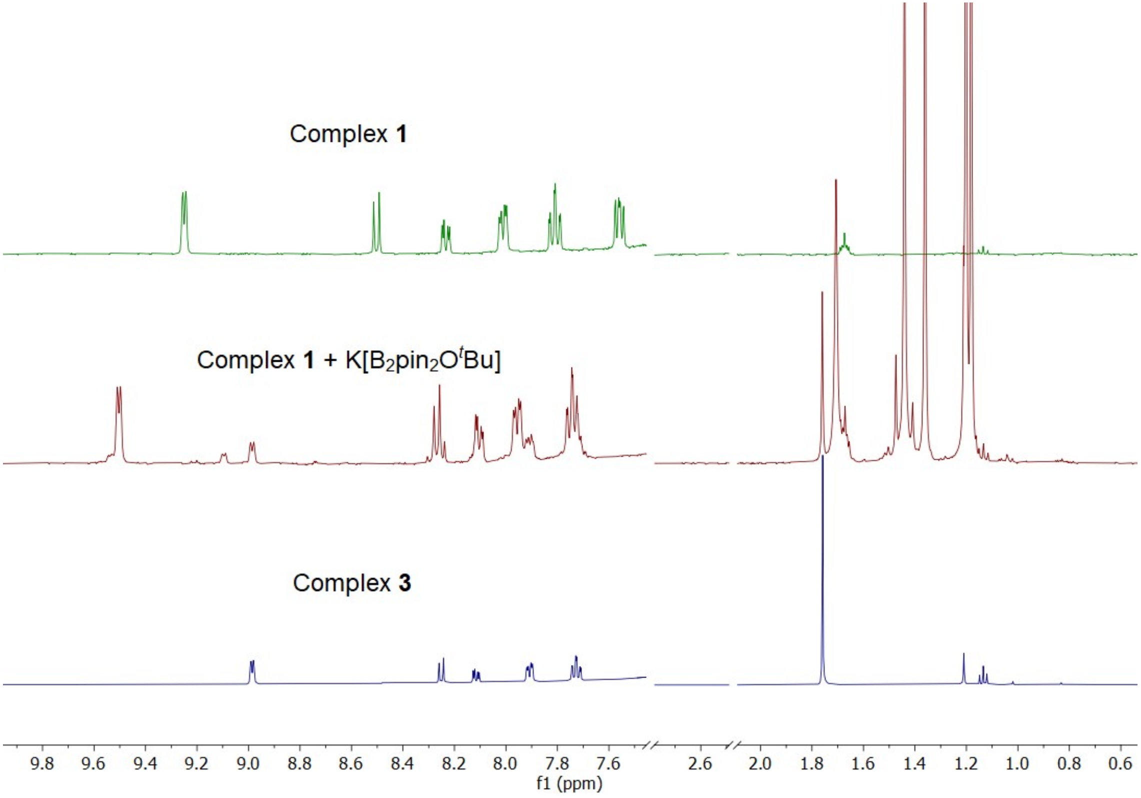

Figure S14. Comparison of the ^1H NMR spectra (*o*-DFB, 400 MHz) of complex **1** (top), **1** + $K[B_2pin_2O^tBu]$ on a 100 mg scale (middle) and complex **3** (bottom, 500 MHz).

Reactivity

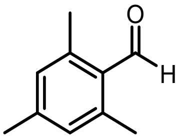	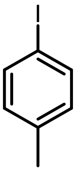	$[TBA][N_3]$	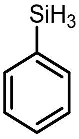	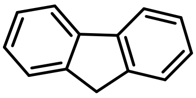
H_2	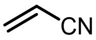	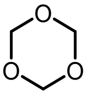	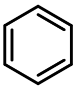	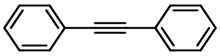

Table S1. Substrates that do not react with **2** or **4** at 25 °C or upon warming (75 °C in the case of THF or 100 °C in the case of *o*-DFB).

Selected examples:

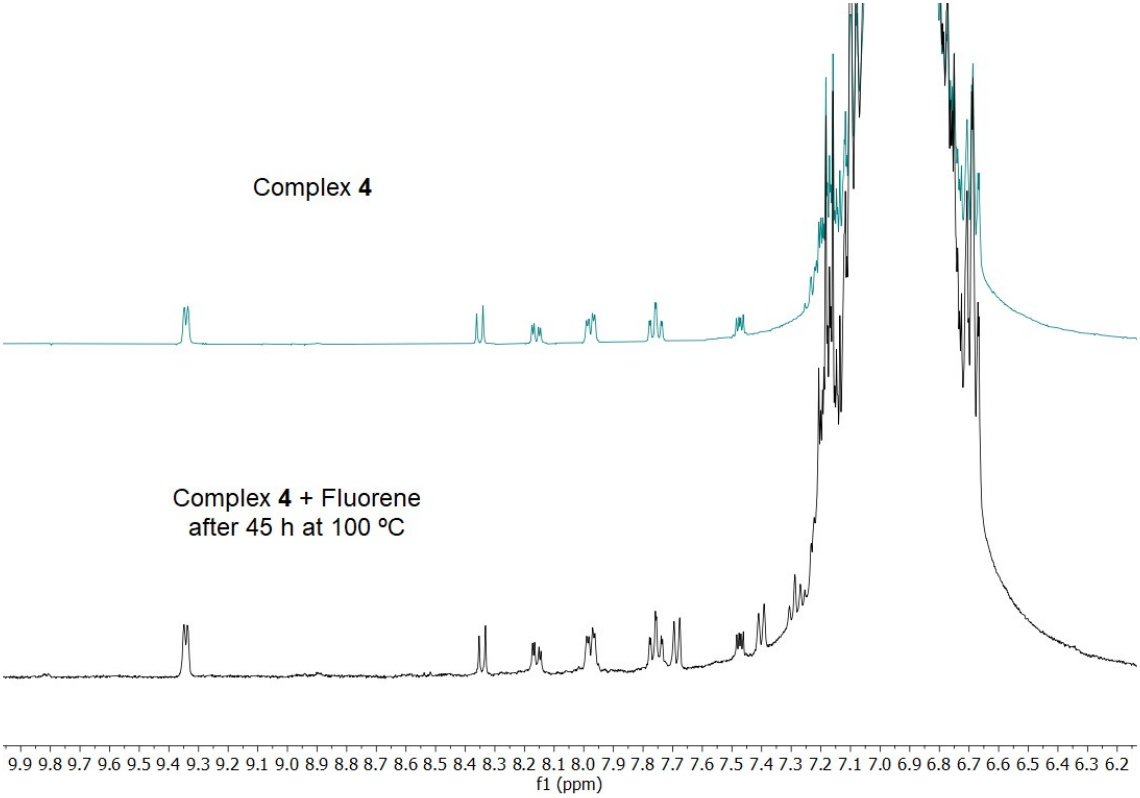

Figure S15. Portion of the ^1H-NMR spectra (*o*-DFB, 400 MHz) of complex **4** (top) and complex **4** + one equivalent of fluorene after 45 h at 100 °C (bottom).

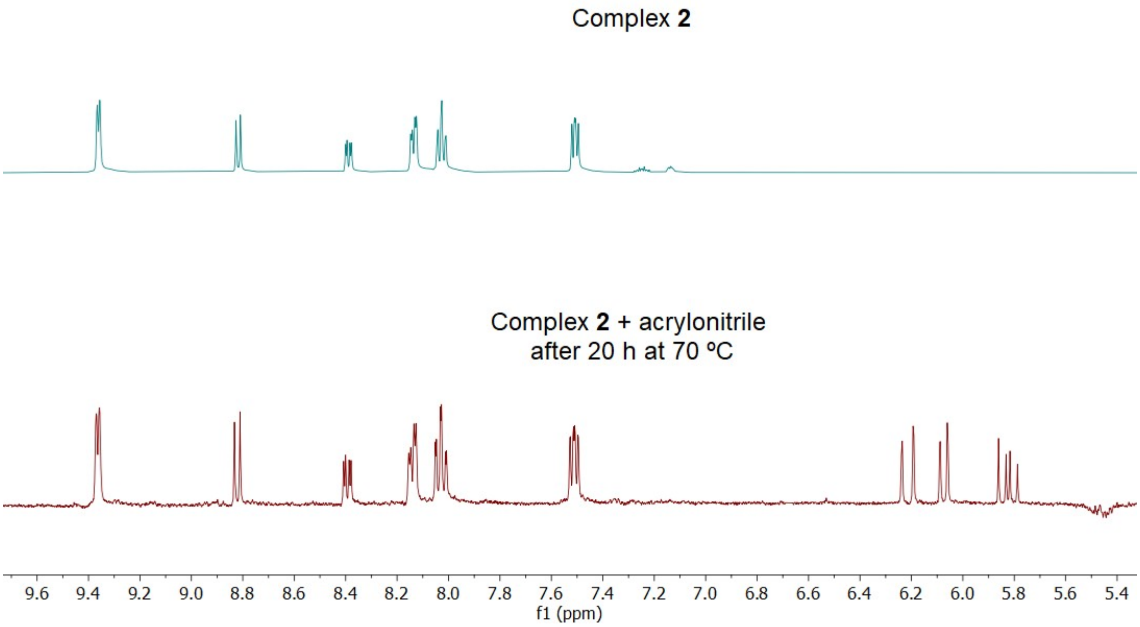

Figure S16. Fragment of the ^{1}H NMR spectra (THF, 400 MHz) of complex **2** (top) and complex **4** + three equivalents of acrylonitrile after 20 h at 70 °C (bottom).

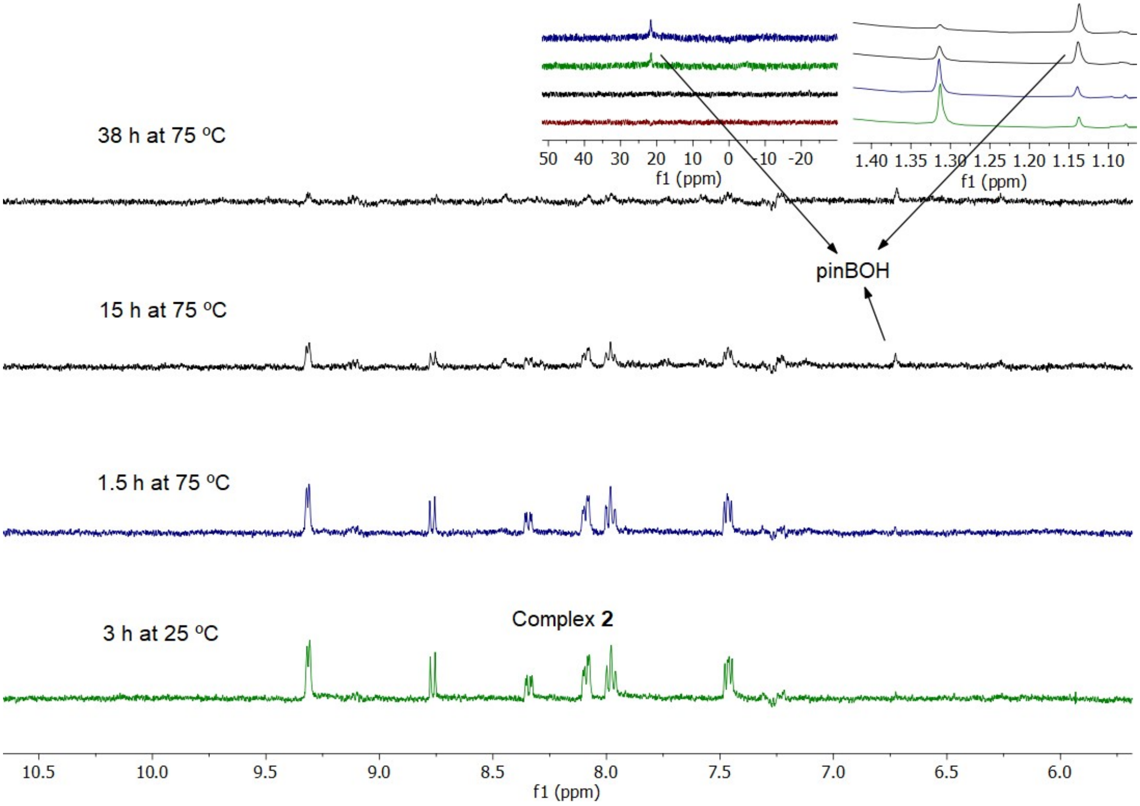

Figure S17. Aromatic region of the ^{1}H NMR spectra (THF, 400 MHz) of the reaction between **2** and O_2 (1 atm). Inset, right: upfield region. Inset, left: ^{11}B NMR spectra (THF, 400 MHz). The new species observed corresponds to pinBOH.[4]

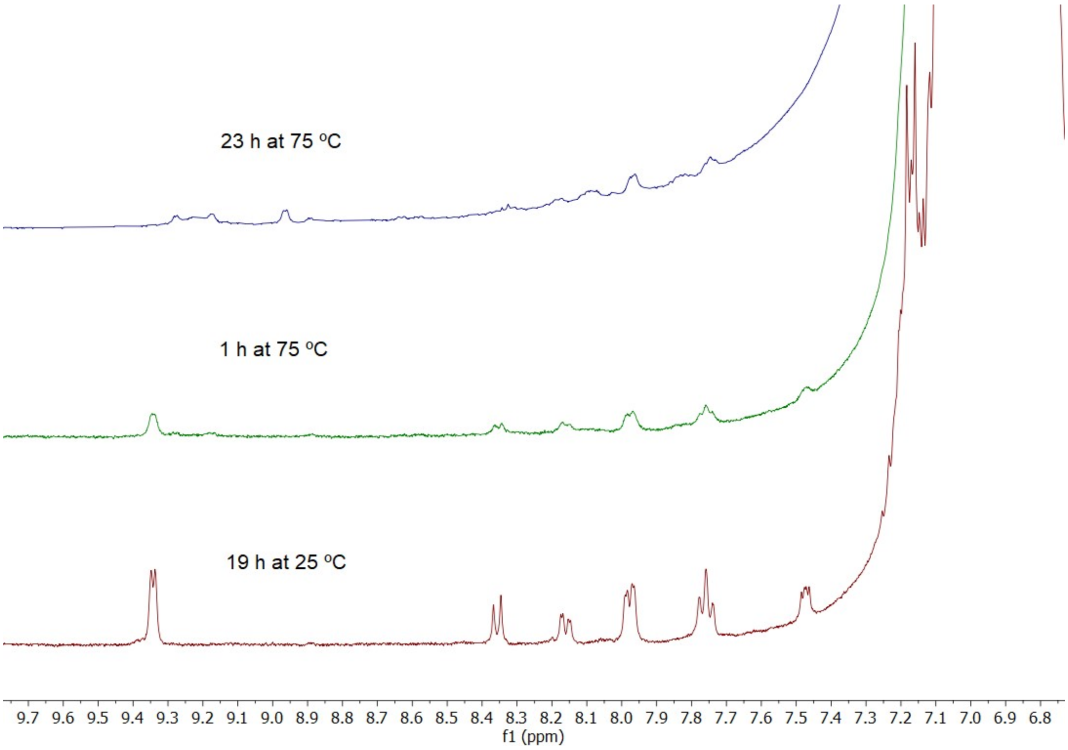

Figure S18. Aromatic region of the ^{1}H NMR spectra (*o*-DFB, 400 MHz) of the reaction between **4** and CO_2 (1 atm). Nothing was observed by ^{11}B NMR.

Reactivity with 4-(trifluoromethyl)phenylacetylene

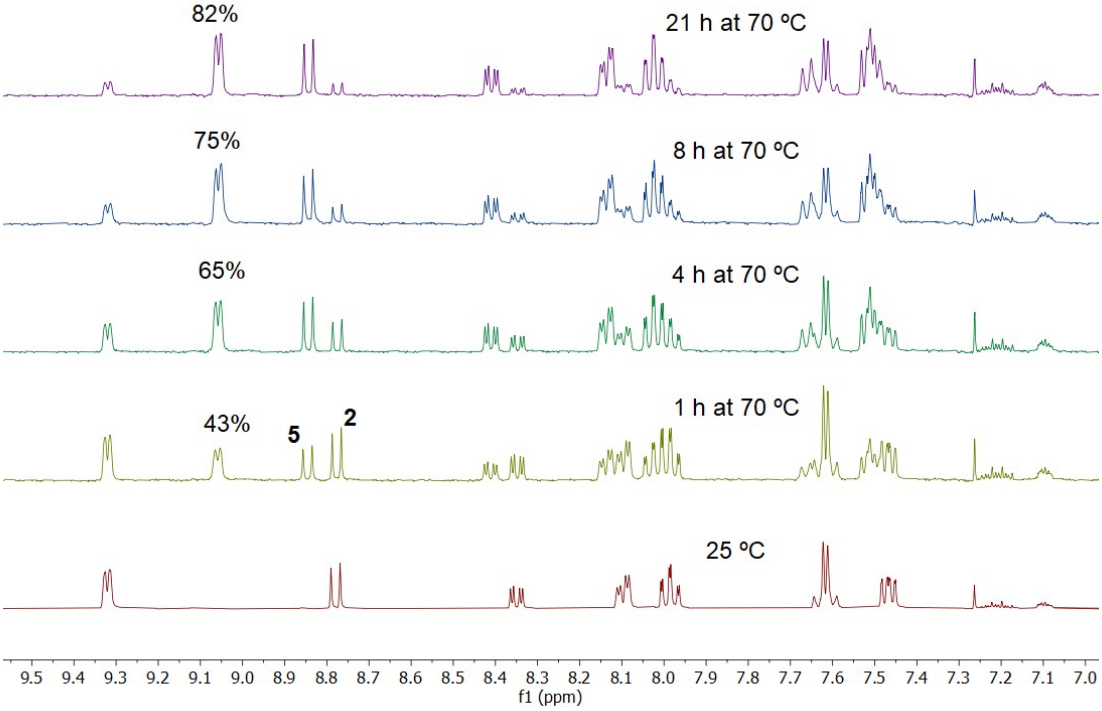

Figure S19. Aromatic region of the ^{1}H NMR spectra (THF, 400 MHz) of the reaction between complex **2** and 4-(trifluoromethyl)phenylacetylene (1.5 equiv). Percentages correspond to the relative ratio of complexes **2** and **5** (integrated to one another).

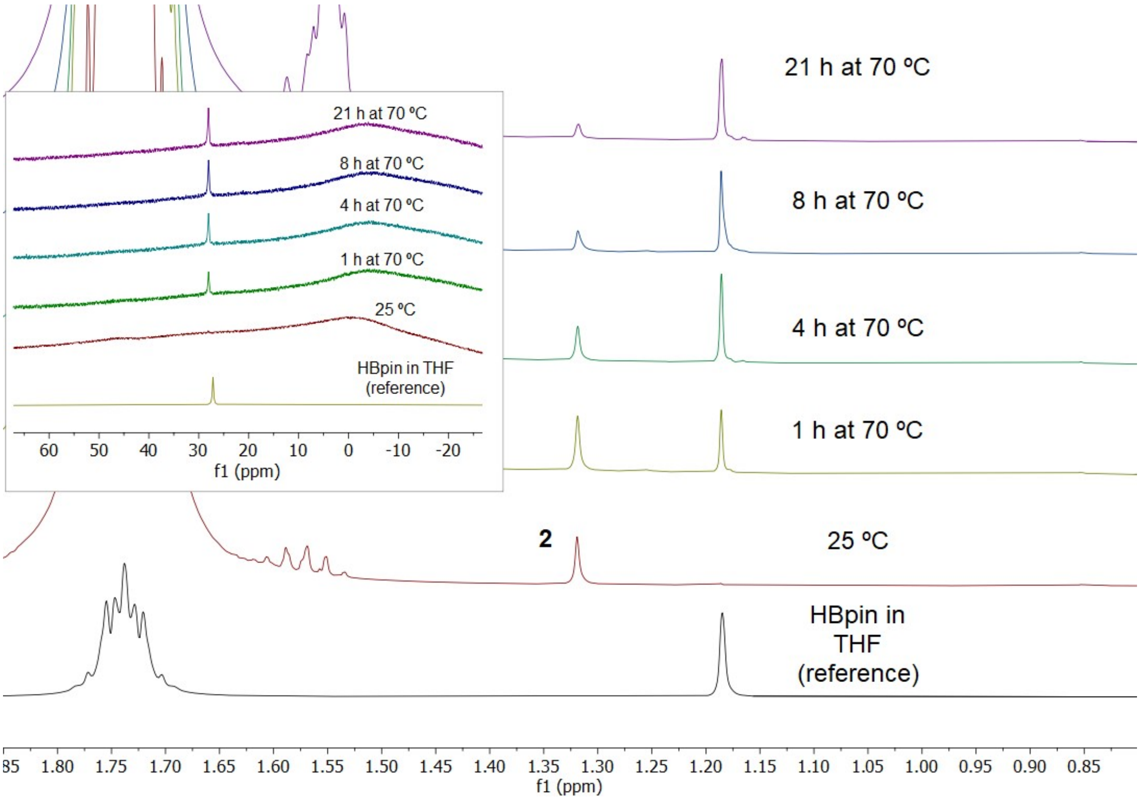

Figure S20. Aliphatic region of the ^{1}H NMR spectra (THF, 400 MHz) of the reaction between complex **2** and 4-(trifluoromethyl)phenylacetylene (1.5 equiv). Inset: ^{11}B NMR spectra. The bottom spectra correspond to HBpin dissolved in THF, as a reference.

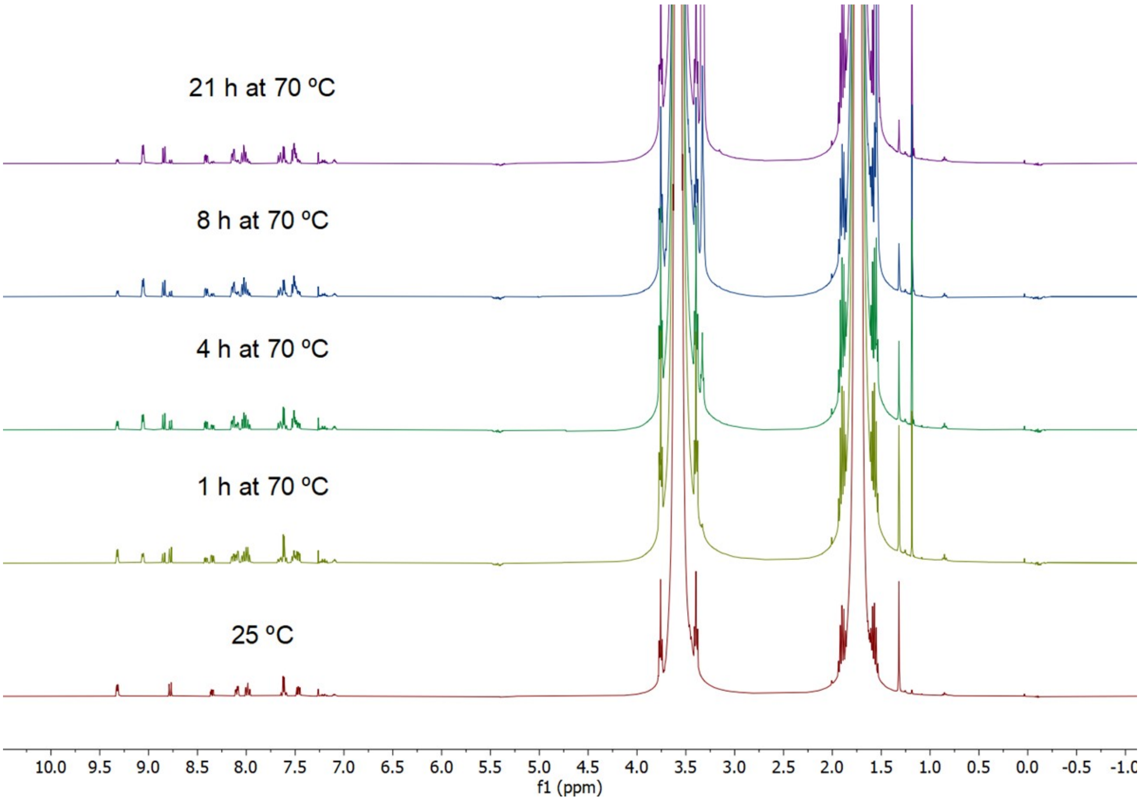

Figure S20A. Full spectral window of the ^{1}H NMR spectra (THF, 400 MHz) of the reaction between complex **2** and 4-(trifluoromethyl)phenylacetylene (1.5 equiv).

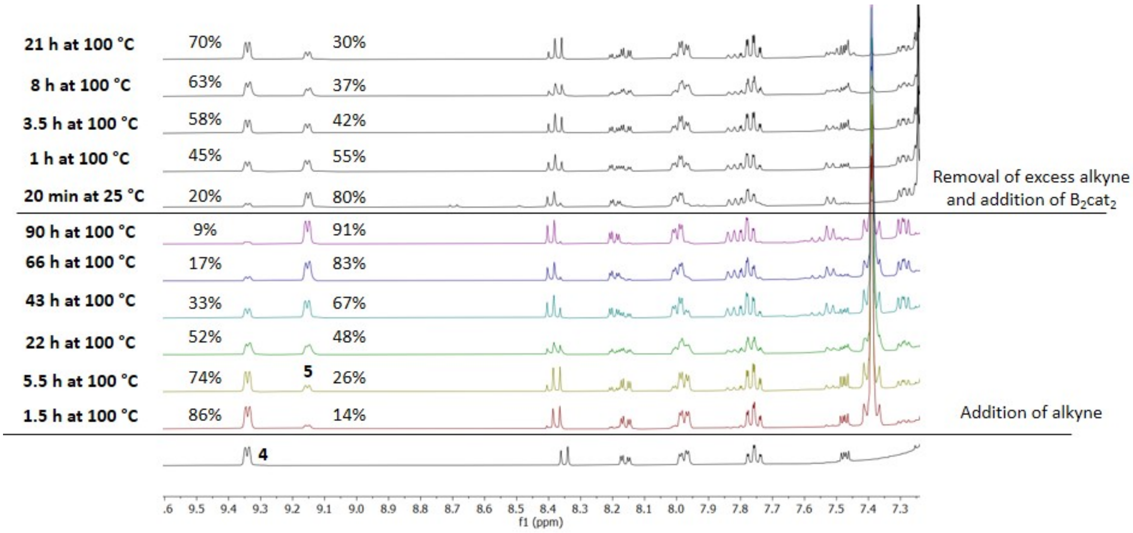

Figure S21. Aromatic region of the ^{1}H NMR spectra (*o*-DFB, 400 MHz) of the reactions between complex **4** and 4-(trifluoromethyl)phenylacetylene (6 equiv, bottom half), and **5** and B$_2$cat$_2$ (6 equiv). Removal of excess alkyne involves evaporating the mixture, washing with pentane (3 x 1 mL) and drying under vacuum. Percentages correspond to the relative ratio of complexes **4** and **5** (integrated to one another).

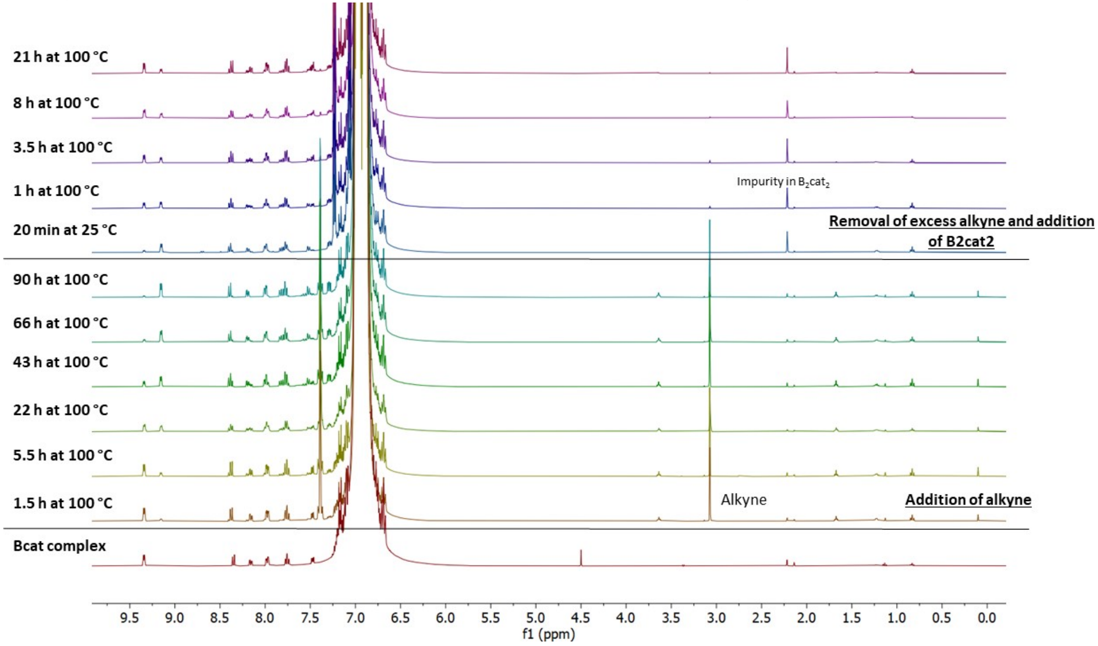

Figure S21A. Full spectral window of the ^{1}H NMR spectra (*o*-DFB, 400 MHz) of the reactions between complex **4** and 4-(trifluoromethyl)phenylacetylene (6 equiv, bottom half), and **5** and B$_2$cat$_2$ (6 equiv). Removal of excess alkyne involves evaporating the mixture, washing with pentane (3 x 1 mL) and drying under vacuum.

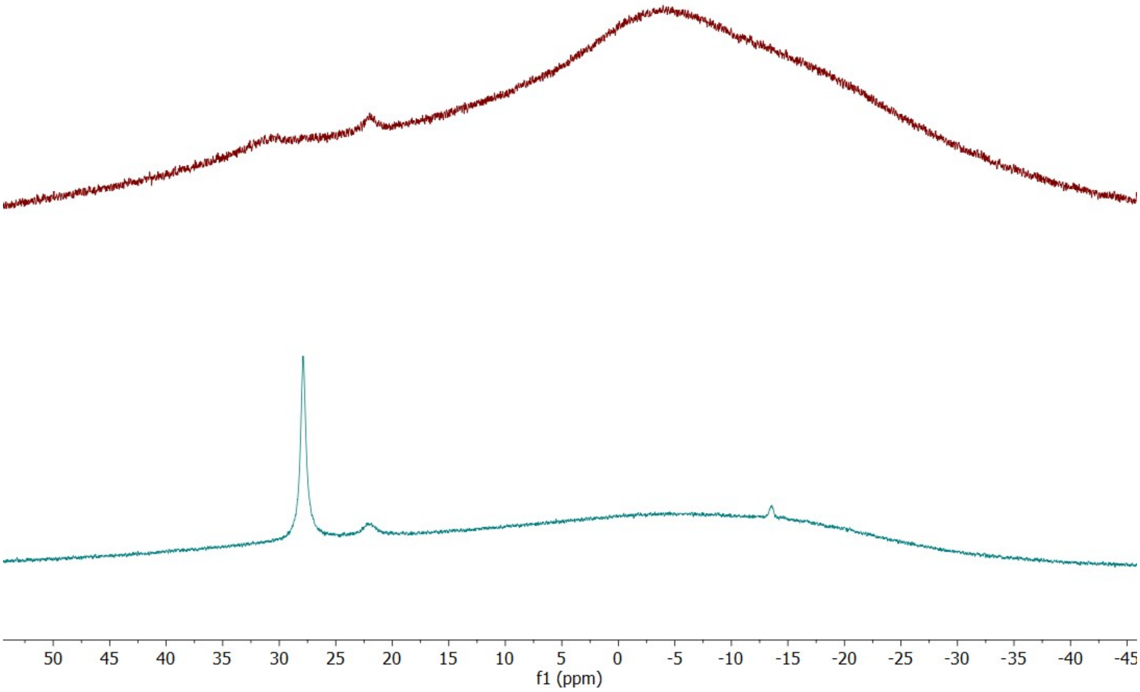

Figure S22. ^{11}B NMR spectra (*o*-DFB, 128 MHz) of: a) reaction between complex **4** and 4-(trifluoromethyl)phenylacetylene (6 equiv) after 90 h at 100 °C (top) and b) HBcat in *o*-DFB (reference sample). The peak observed in the top spectrum (presumably catBOBcat)[5] is already present in a fresh sample of HBcat.

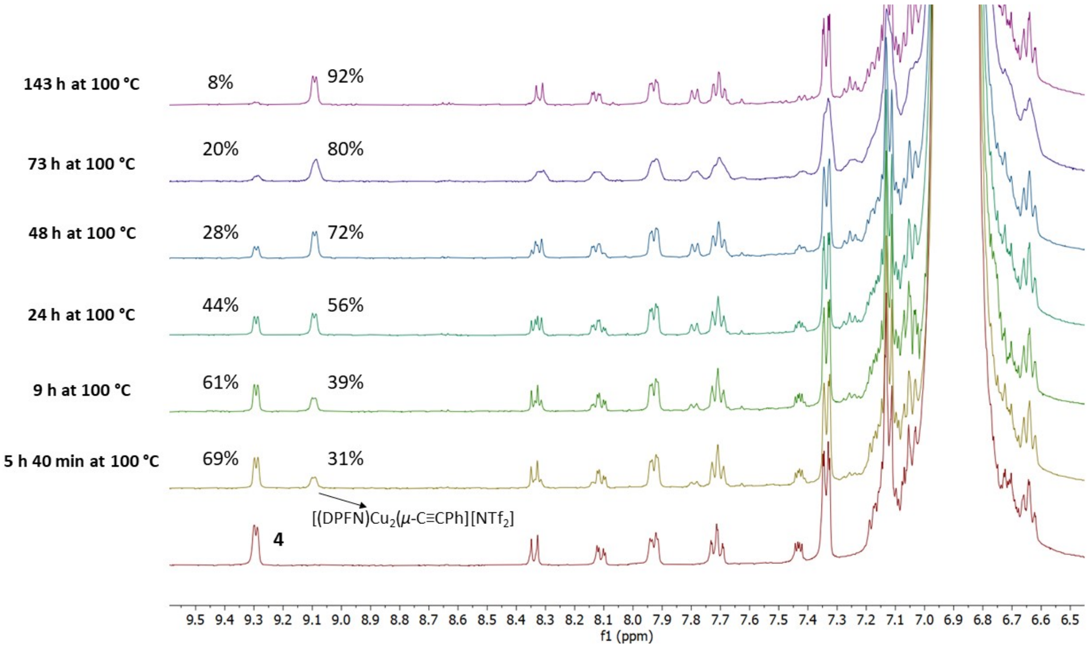

Figure S23. Aromatic region of the ^{1}H NMR spectra (*o*-DFB, 400 MHz) of the reactions between complex **4** and phenylacetylene (6 equiv). While the reaction rate is similar to that observed in Figure S21, high conversions (≥ 80%) require longer times in this case. Percentages correspond to the relative ratio of complexes **4** and **[(DPFN)Cu$_2$(μ-C≡CPh][NTf$_2$]** (integrated to one another).

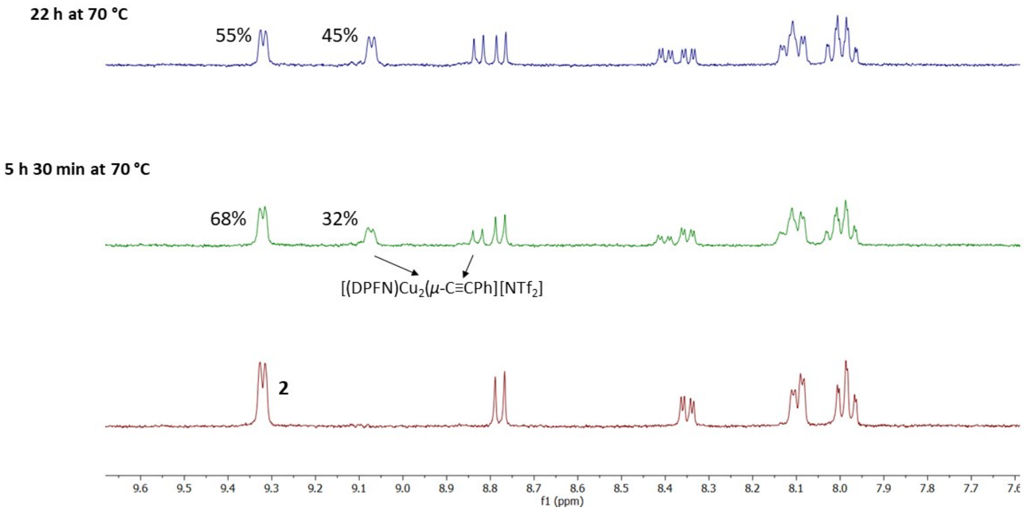

Figure S24. Fragment of the aromatic region of the ^{1}H NMR spectra (THF, 400 MHz) of the reaction between complex **2** and phenylacetylene (1.5 equiv). Percentages correspond to the relative ratio of complexes **2** and **[(DPFN)Cu$_2$(μ-C≡CPh][NTf$_2$]** (integrated to one another).

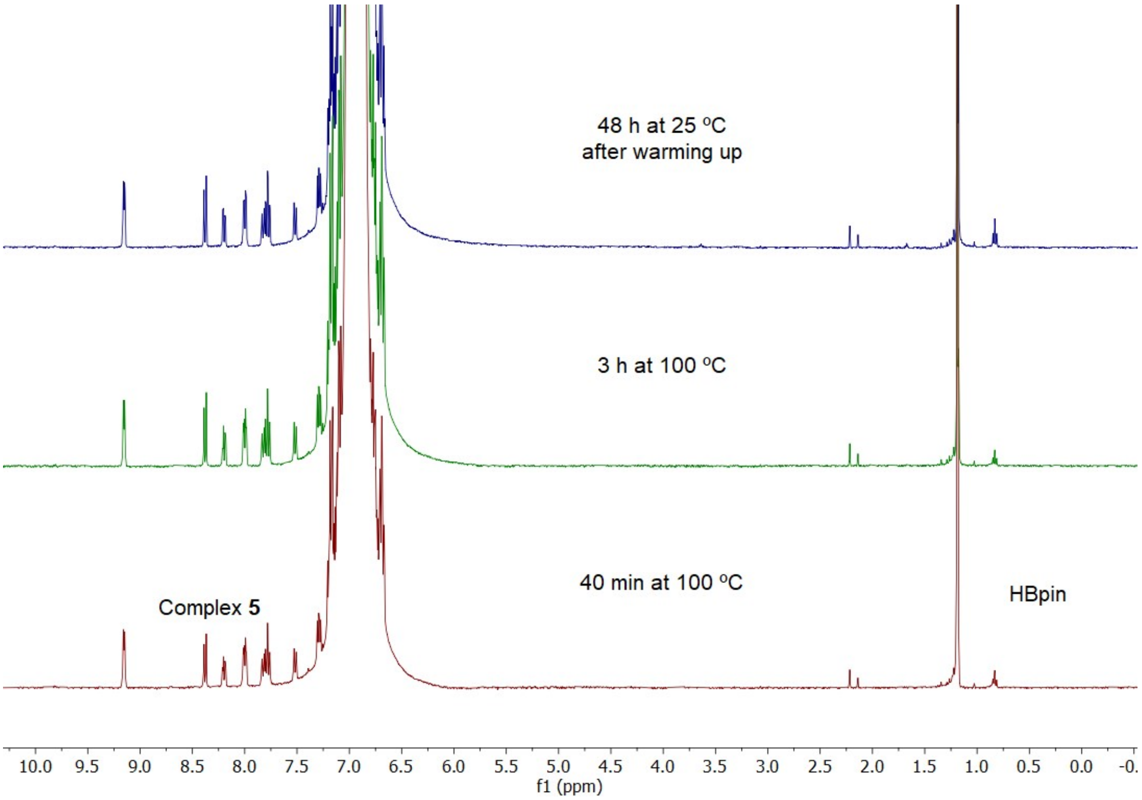

Figure S25. ^{1}H NMR spectra (*o*-DFB, 400 MHz) of the control experiment between complex **5** and HBpin (1 equiv).

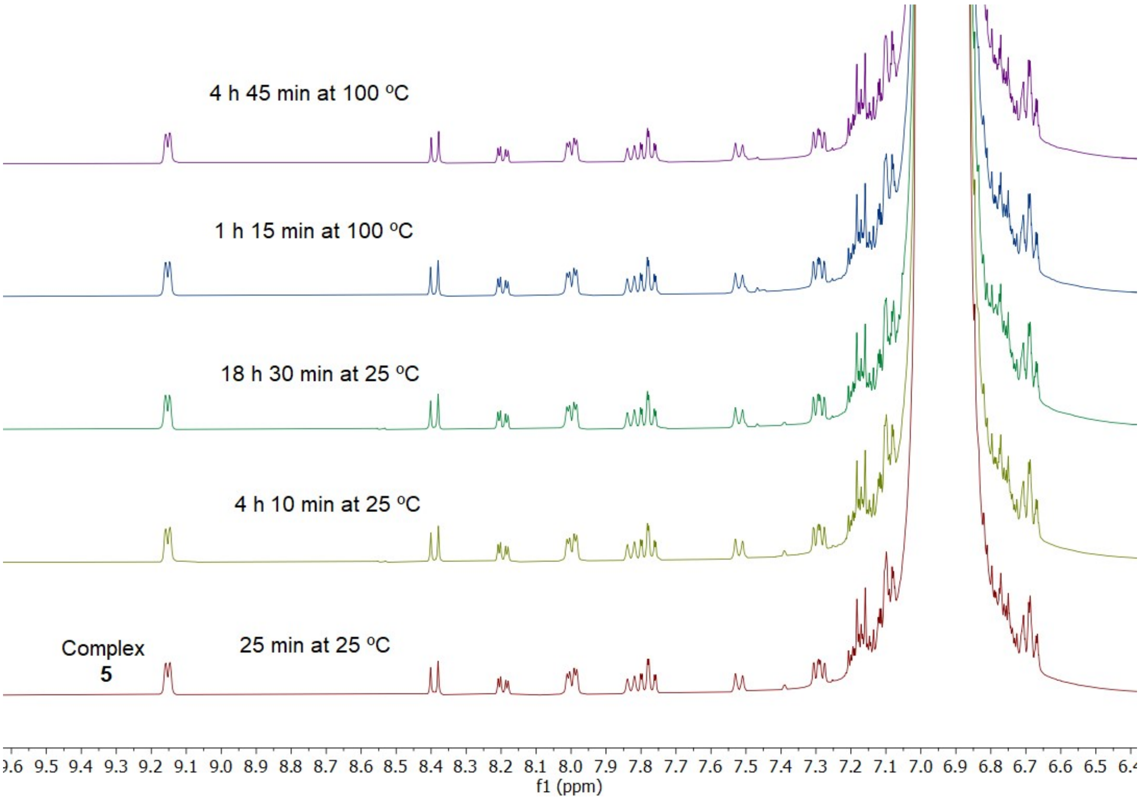

Figure S26. Aromatic region of the ^{1}H NMR spectra (*o*-DFB, 400 MHz) of the control experiment between complex **5** and HBcat (1 equiv). HBcat resonances overlap with those of *o*-DFB.

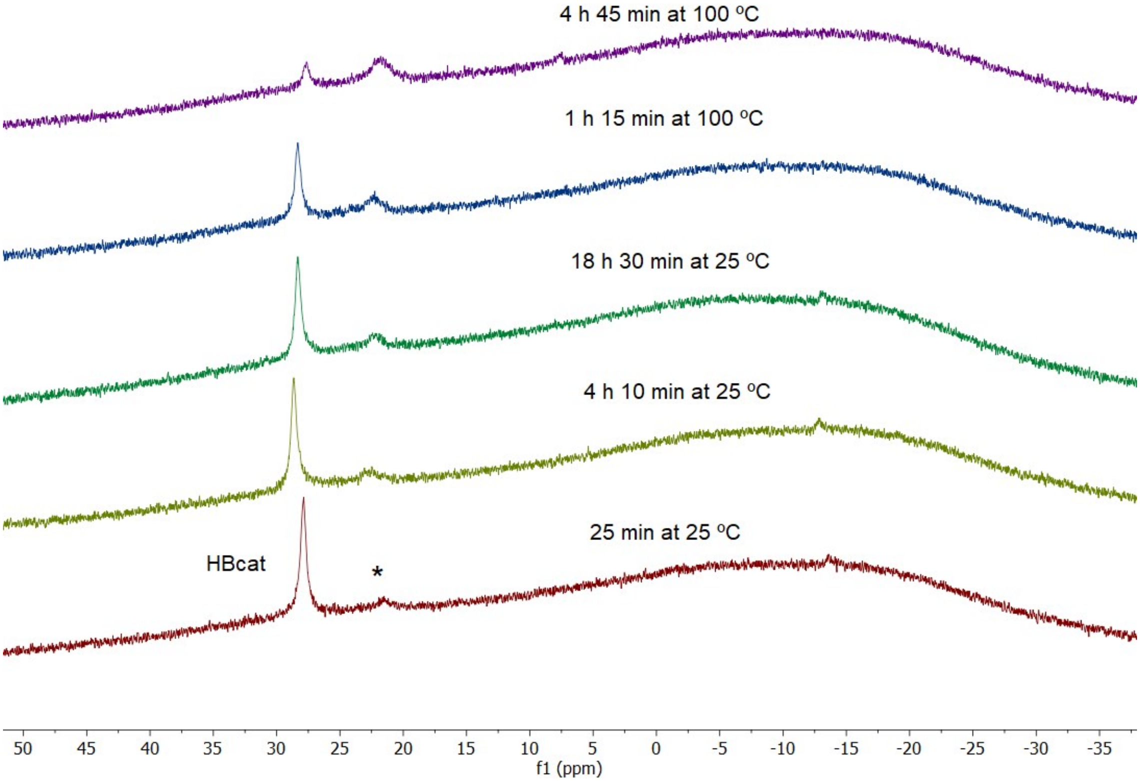

Figure S27. ^{11}B NMR spectra (*o*-DFB, 128 MHz) of the control experiment between complex **5** and HBcat (1 equiv). HBcat seems to decompose to species * (presumably catBOBcat).[4]

4. Mass spectra

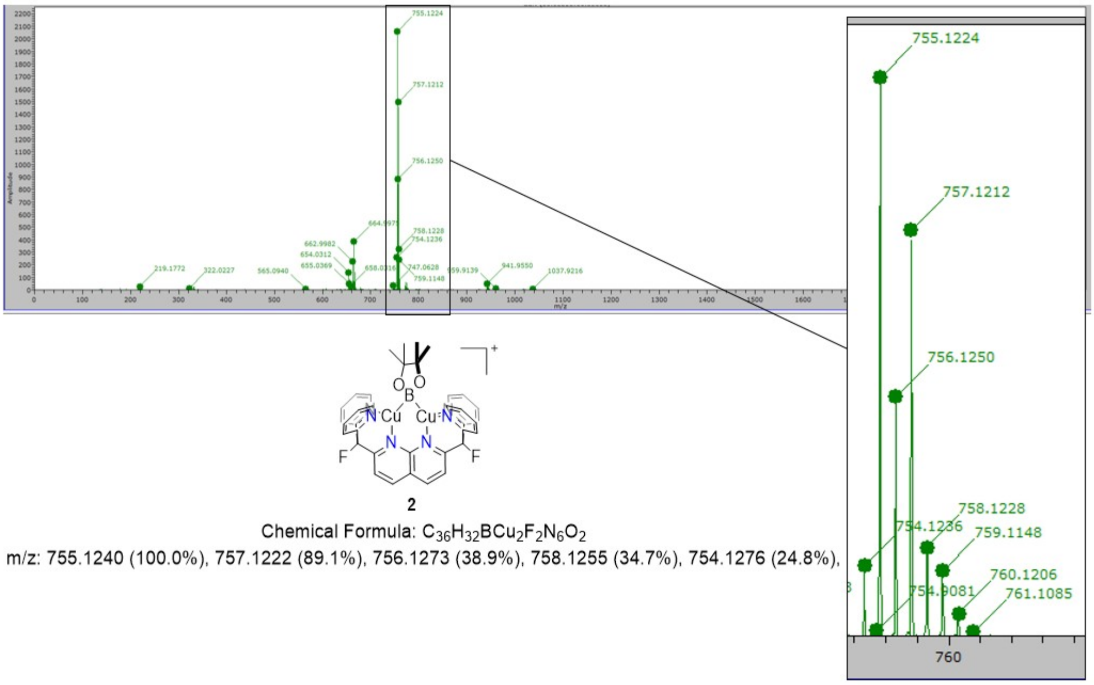

Figure S28. Mass spectrum of complex **2**.

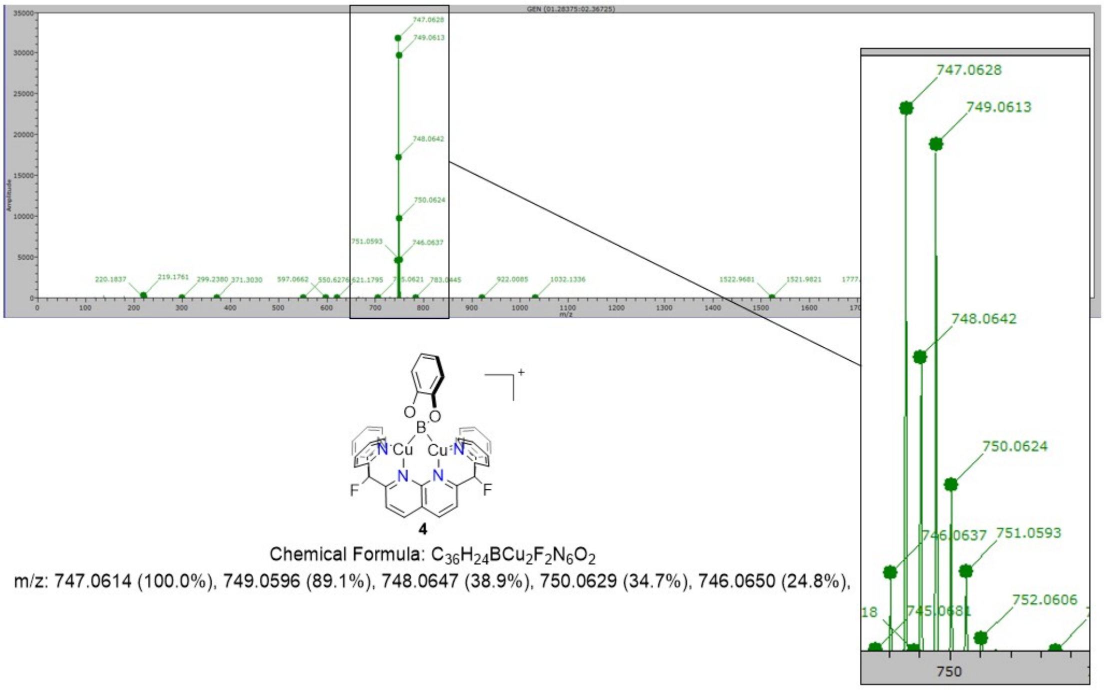

Figure S29. Mass spectrum of complex **4**.

5. IR spectra

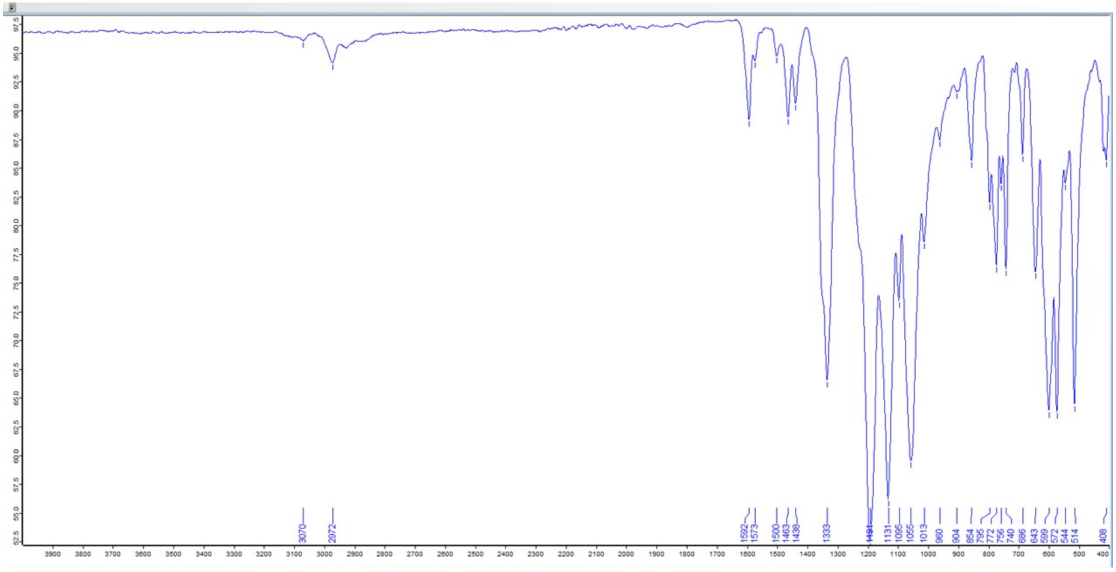

Figure S30. IR spectrum of complex **2**.

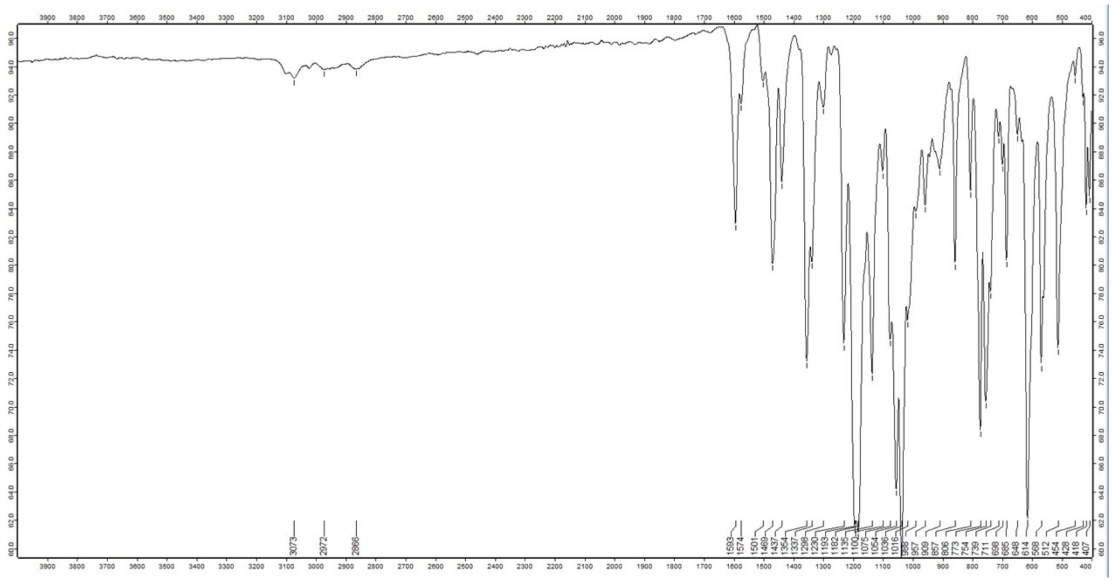

Figure S31. IR spectrum of complex **4**.

6. % Buried Volume Calculations

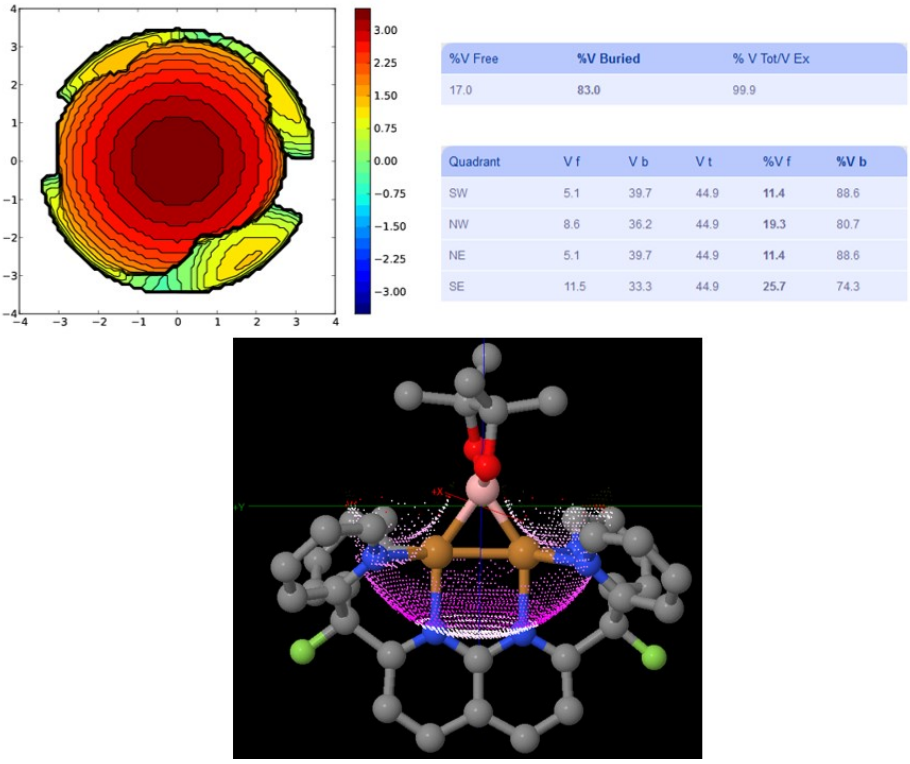

%V Free	%V Buried	% V Tot/V Ex
17.0	83.0	99.9

Quadrant	V f	V b	V t	%V f	%V b
SW	5.1	39.7	44.9	11.4	88.6
NW	8.6	36.2	44.9	19.3	80.7
NE	5.1	39.7	44.9	11.4	88.6
SE	11.5	33.3	44.9	25.7	74.3

Figure S32. % Buried Volume on B in complex **2**.

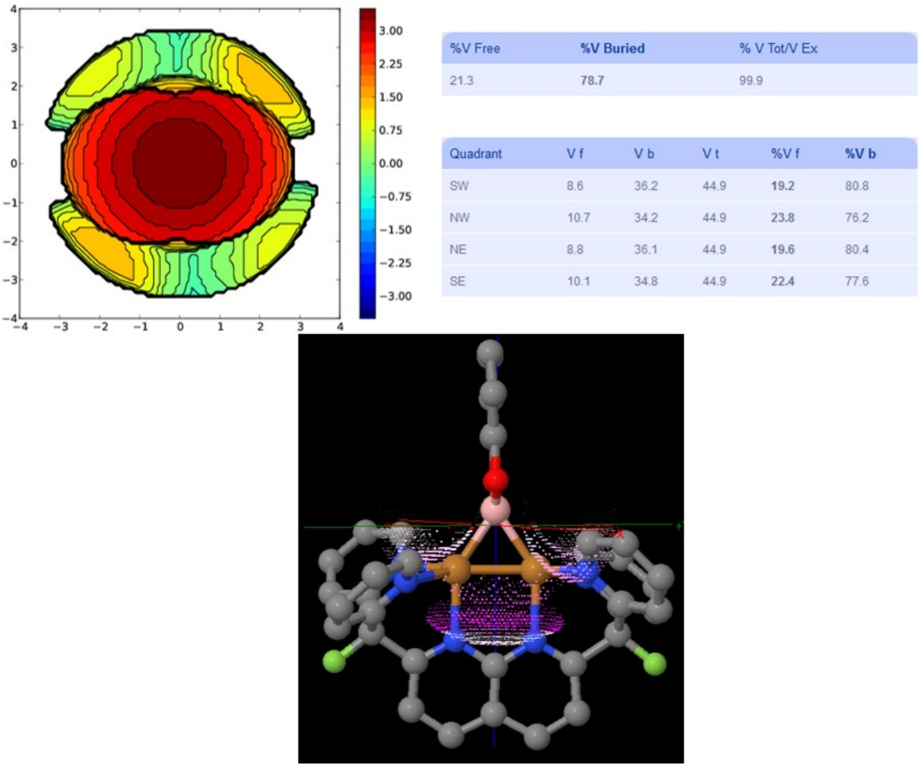

%V Free	%V Buried	% V Tot/V Ex
21.3	78.7	99.9

Quadrant	V f	V b	V t	%V f	%V b
SW	8.6	36.2	44.9	19.2	80.8
NW	10.7	34.2	44.9	23.8	76.2
NE	8.8	36.1	44.9	19.6	80.4
SE	10.1	34.8	44.9	22.4	77.6

Figure S33. % Buried Volume on B in complex **4**.

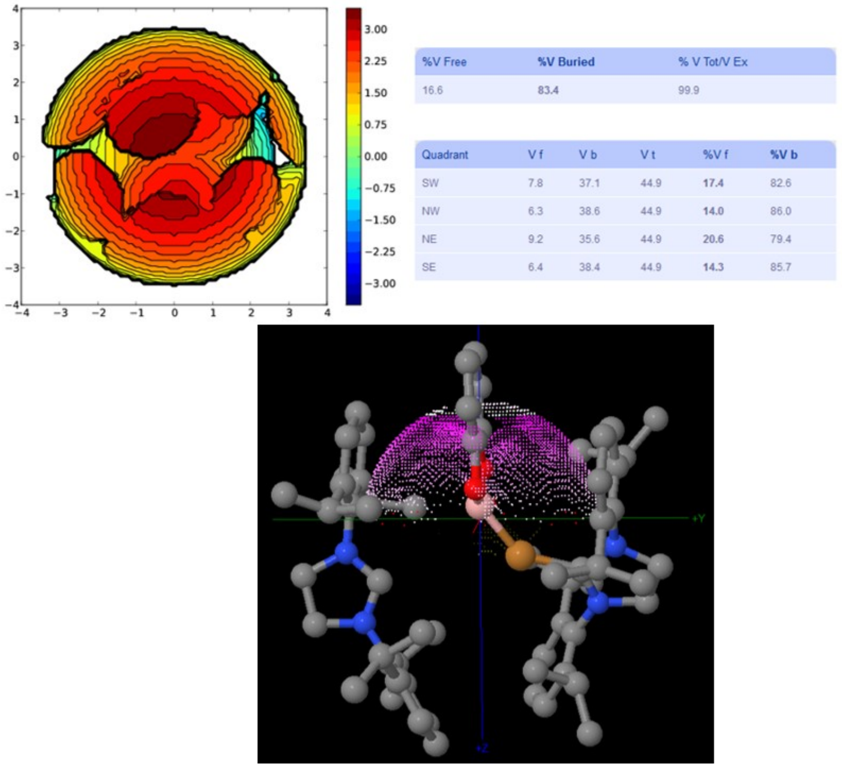

%V Free	%V Buried	% V Tot/V Ex
16.6	83.4	99.9

Quadrant	V f	V b	V t	%V f	%V b
SW	7.8	37.1	44.9	**17.4**	82.6
NW	6.3	38.6	44.9	**14.0**	86.0
NE	9.2	35.6	44.9	**20.6**	79.4
SE	6.4	38.4	44.9	**14.3**	85.7

Figure S34. % Buried Volume on B in {[(SIPr)Cu]$_2$(μ-Bcat)}{BF$_4$}.

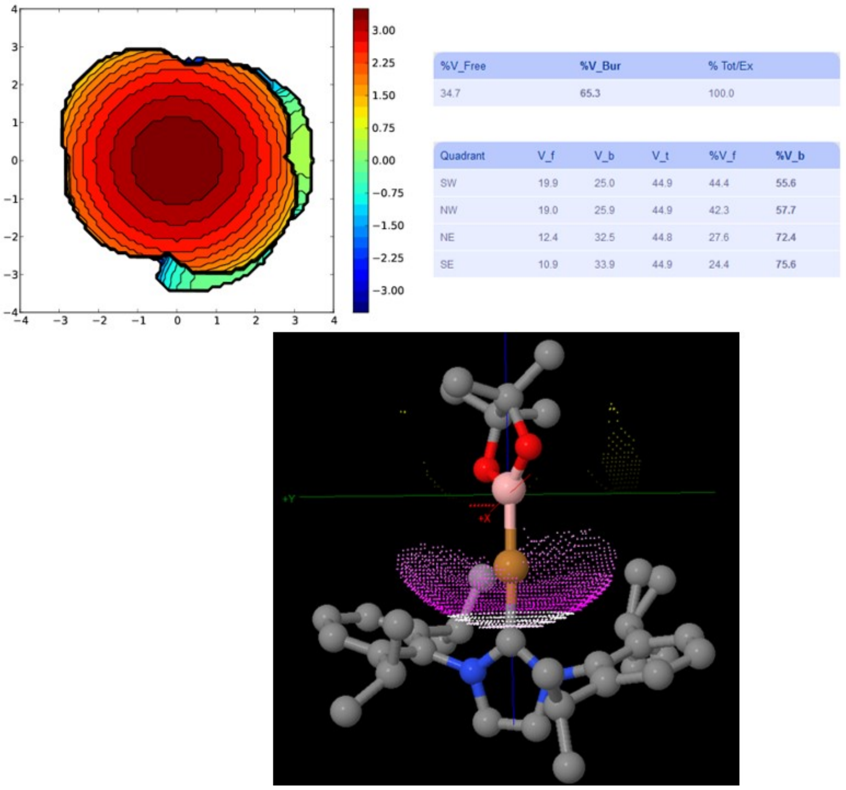

%V_Free	%V_Bur	% Tot/Ex
34.7	65.3	100.0

Quadrant	V_f	V_b	V_t	%V_f	%V_b
SW	19.9	25.0	44.9	44.4	**55.6**
NW	19.0	25.9	44.9	42.3	**57.7**
NE	12.4	32.5	44.8	27.6	**72.4**
SE	10.9	33.9	44.9	24.4	**75.6**

Figure S35. % Buried Volume on B in (IPr)CuBpin.

6. Computational Details

DFT calculations were performed at the Molecular Graphics and Computation Facility of the University of California, Berkeley, using the Gaussian 16 suite of programs.[6] The geometry of the $[(DPFN)Cu_2(\mu\text{-Bpin})]^+$ and $[(DPFN)Cu_2(\mu\text{-Bcat})]^+$ fragments was optimized in the gas phase without restrictions using the PBE0 functional,[7] as implemented in the G16 software along with Grimme's dispersion correction with Becke-Johnson damping function (D3(BJ)).[8] Non-metal atoms were described with the 6-31g(d,p) basis set[9] and the Cu atoms were modelled with the Stuttgart/Dresden SDD basis set and its associated effective core potential.[10] Vibrational analysis was used to characterize the stationary point in the potential energy surface. Natural Bond Order (NBO) and Natural Localized Molecular Orbital (NLMO) analyses were performed on the optimized structure using NBO 6.0[11] Structure and orbital visualization was performed with Chemcraft software.[12] QTAIM analysis was conducted with Multiwfn software.[13]

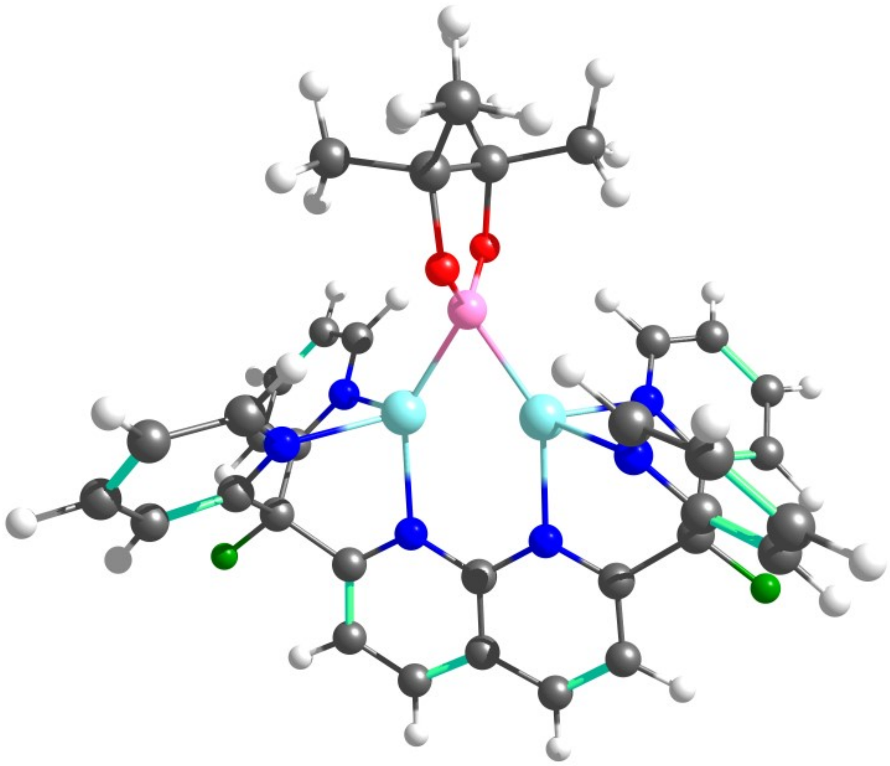

Figure S36. Optimized geometry of complex **2**.

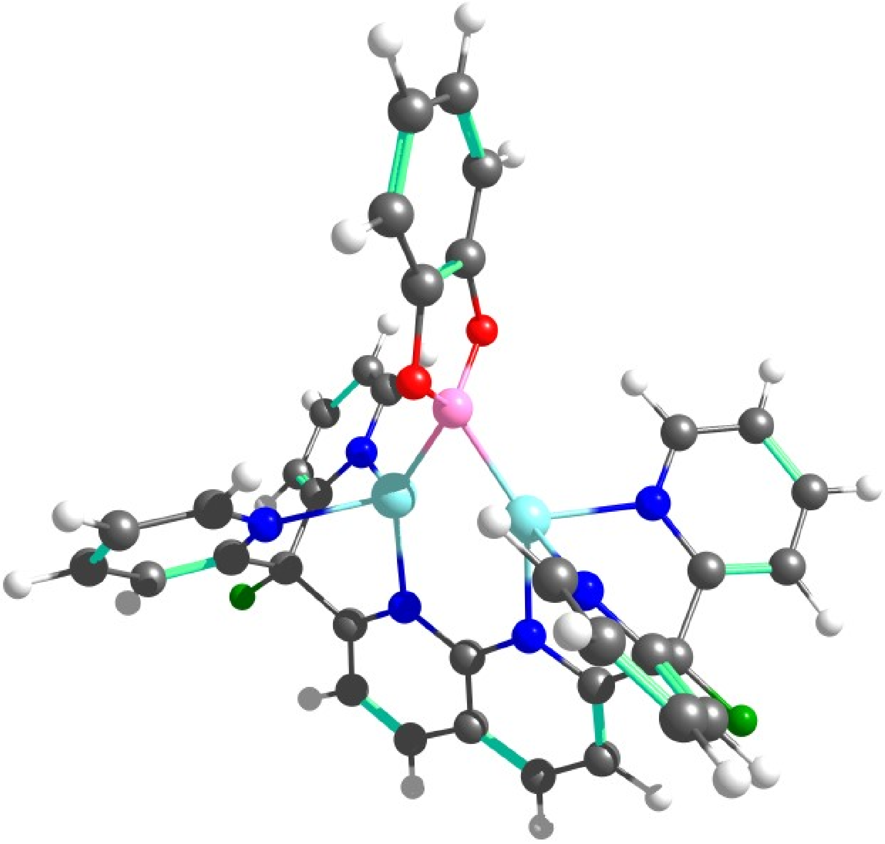

Figure S37. Optimized geometry of complex **4**.

	Complex **2**		Complex **4**	
Parameter	Experimental[a]	Calculated	Experimental	Calculated
Cu–Cu	2.326(1)/2.3187(9) Å	2.31704 Å	2.3220(9) Å	2.32711 Å
Cu–B–Cu	68.0(2)/67.4(2)°	68.105°	68.2(2)°	69.121°
Cu(1)–B	2.075(6)/2.089(6) Å	2.06896 Å	2.068(7) Å	2.05111 Å
Cu(2)–B	2.081(6)/2.089(7) Å	2.06897 Å	2.074(6) Å	2.05116 Å
B–O(1)	1.406(8)/1.409(8) Å	1.40356 Å	1.425(8) Å	1.43138 Å
B–O(2)	1.403(7)/1.380(9) Å	1.40356 Å	1.429(8) Å	1.43121 Å
Cu–Cu–B–O	113.5(5)/116.0(5)°	110.850°	112.5(5) °	113.061°

Table S2. Comparison of calculated and experimental structural parameters for complexes **2** and **4**.[a] 2 molecules were observed in the asymmetric unit.

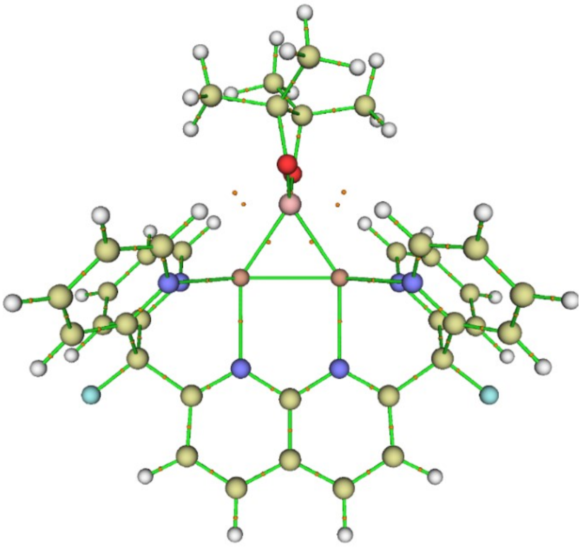

Figure S38. Topological analysis of complex **2** and its computed (3,-1) critical points.

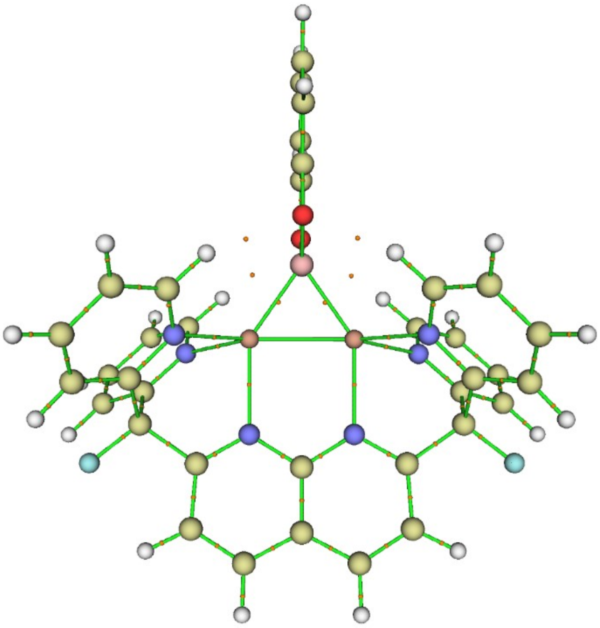

Figure S39. Topological analysis of complex **4** and its computed (3,-1) critical points.

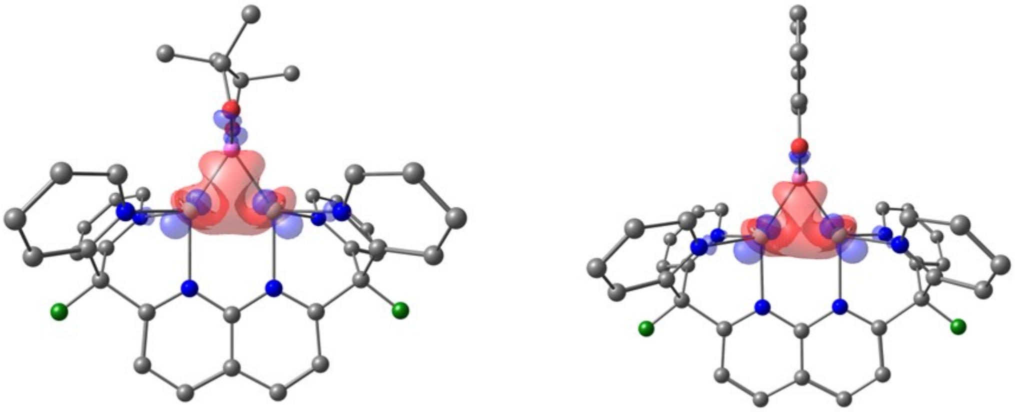

Complex 2

HOMO-1
(-5.58 eV, -128.7 kcal mol^{-1})

HOMO-(HOMO-1) energy difference:
0.17 eV (3.92 kcal mol^{-1})

Complex 4

HOMO-2
(-5.94 eV, -137.0 kcal mol^{-1})

HOMO-(HOMO-2) energy difference:
0.30 eV (6.92 kcal mol^{-1})

Figure S40. Selected molecular orbitals of complexes **2** and **4**, describing the bonding of the Cu−B−Cu fragment.

7. Selected Natural Localized Molecular Orbitals

Complex **2**

```
Hybridization/Polarization Analysis of NLMOs in NAO Basis:
 NLMO / Occupancy / Percent from Parent NBO / Atomic Hybrid Contributions
 ------------------------------------------------------------------------------
164. (2.00000)  82.9871% BD ( 1)Cu 59- B 63

                        14.913% Cu 59 s( 97.72%)p 0.01(  1.00%)d 0.01(  1.29%)
                        14.761% Cu 60 s( 97.78%)p 0.01(  1.01%)d 0.01(  1.21%)
                        68.118%  B 63 s( 50.18%)p 0.99( 49.80%)d 0.00(  0.02%)
```

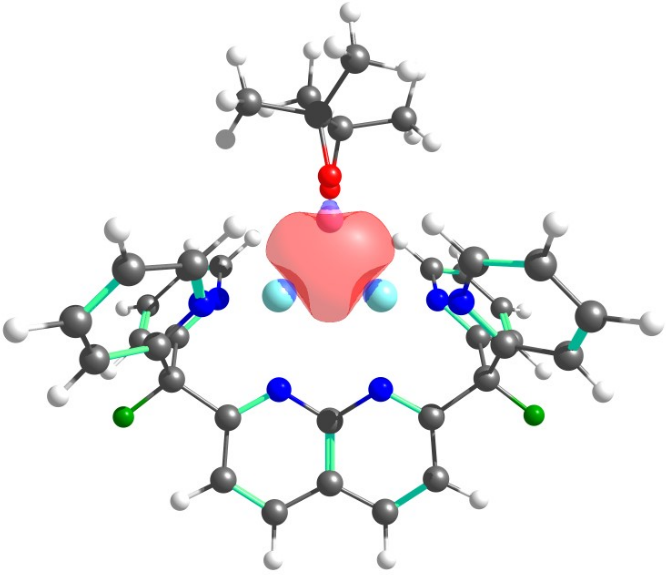

Figure S41. NLMO 164 of complex **2**.

Complex **4**

```
Hybridization/Polarization Analysis of NLMOs in NAO Basis:
 NLMO / Occupancy / Percent from Parent NBO / Atomic Hybrid Contributions
 ------------------------------------------------------------------------------
164. (2.00000)  83.8071% BD ( 1)Cu 59- B 73

                         14.396% Cu 59 s( 97.82%)p 0.01(  0.89%)d 0.01(  1.29%)
                         14.203% Cu 60 s( 97.92%)p 0.01(  0.90%)d 0.01(  1.18%)
                         69.461%  B 73 s( 54.56%)p 0.83( 45.42%)d 0.00(  0.02%)
```

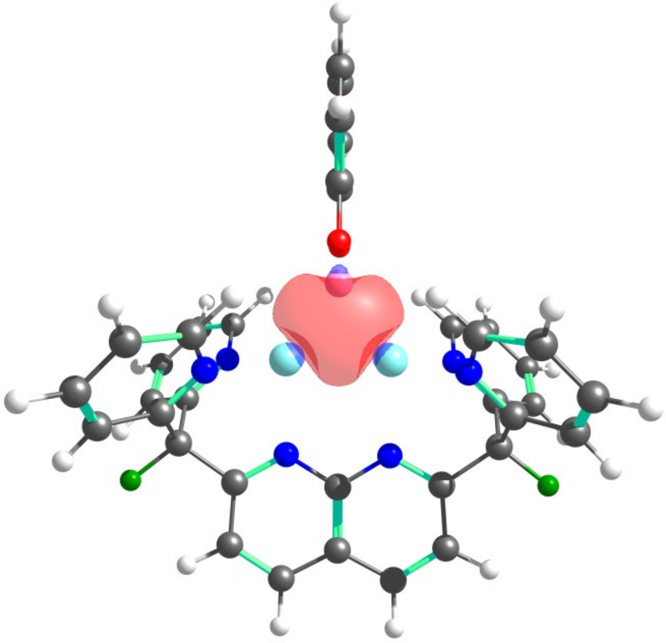

Figure S42. NLMO 164 of complex **4**.

8. Cartesian Coordinates of the optimized structures

Complex **2**

C	-2.302337000	-2.540755000	-0.017018000
C	-2.407199000	-3.949327000	-0.018725000
H	-3.380815000	-4.421510000	-0.025128000
C	-1.251712000	-4.689925000	-0.011428000
H	-1.285088000	-5.775785000	-0.012906000
C	-0.000107000	-4.032813000	0.000412000
C	-0.000075000	-2.616531000	0.000207000
C	1.251467000	-4.689980000	0.012437000
H	1.284791000	-5.775842000	0.014233000
C	2.406988000	-3.949435000	0.019499000
H	3.380582000	-4.421663000	0.026021000
C	2.302194000	-2.540858000	0.017382000
C	3.556487000	-1.668726000	0.013862000
C	3.641816000	-0.817371000	-1.254934000
C	4.679852000	-0.997627000	-2.162817000
H	5.440098000	-1.748750000	-1.989441000
C	4.709655000	-0.184899000	-3.291806000
H	5.506128000	-0.298690000	-4.021140000
C	3.714600000	0.770100000	-3.473425000
H	3.708084000	1.421756000	-4.340694000
C	2.716565000	0.876800000	-2.513590000
H	1.911241000	1.602963000	-2.588995000
C	3.656636000	-0.804998000	1.272961000
C	4.715221000	-0.969322000	2.159940000
H	5.473698000	-1.720199000	1.978534000
C	4.769445000	-0.142197000	3.277167000
H	5.582733000	-0.244692000	3.989354000
C	3.777387000	0.813955000	3.467869000
H	3.789343000	1.478789000	4.324935000
C	2.757230000	0.904811000	2.530516000
H	1.954437000	1.632290000	2.617672000
C	-3.556589000	-1.668565000	-0.013776000
C	-3.656574000	-0.805066000	-1.273046000
C	-4.715012000	-0.969593000	-2.160163000
H	-5.473488000	-1.720467000	-1.978744000
C	-4.769095000	-0.142670000	-3.277546000
H	-5.582269000	-0.245326000	-3.989840000
C	-3.777047000	0.813489000	-3.468264000
H	-3.788900000	1.478172000	-4.325449000
C	-2.757037000	0.904547000	-2.530772000
H	-1.954258000	1.632042000	-2.617940000
C	-3.641992000	-0.816986000	1.254864000
C	-4.680160000	-0.996984000	2.162647000
H	-5.440464000	-1.748053000	1.989295000

C	-4.710012000	-0.184076000	3.291505000
H	-5.506587000	-0.297666000	4.020760000
C	-3.714872000	0.770840000	3.473098000
H	-3.708388000	1.422628000	4.340267000
C	-2.716708000	0.877280000	2.513368000
H	-1.911312000	1.603364000	2.588757000
N	1.150124000	-1.904035000	0.011289000
N	-1.150239000	-1.903981000	-0.011079000
N	2.684801000	0.095330000	-1.429797000
N	2.699871000	0.107496000	1.458505000
N	-2.699811000	0.107426000	-1.458611000
N	-2.684897000	0.095637000	1.429701000
F	4.645229000	-2.520016000	0.012241000
F	-4.645374000	-2.519801000	-0.012105000
Cu	1.157874000	0.215658000	0.038384000
Cu	-1.157892000	0.215736000	-0.038414000
C	0.288848000	4.105821000	-0.722846000
C	-0.288598000	4.105854000	0.722755000
B	0.000046000	1.929888000	-0.000029000
O	0.063586000	2.744868000	-1.140972000
O	-0.063424000	2.744894000	1.140902000
C	1.795774000	4.342332000	-0.758652000
H	2.164621000	4.136999000	-1.768197000
H	2.051598000	5.376318000	-0.507429000
H	2.314375000	3.672748000	-0.065295000
C	-0.411020000	5.041260000	-1.690499000
H	-0.327022000	6.081351000	-1.358226000
H	0.053354000	4.964749000	-2.678875000
H	-1.469733000	4.792287000	-1.793209000
C	0.411427000	5.041232000	1.690343000
H	0.327474000	6.081328000	1.358077000
H	-0.052855000	4.964750000	2.678765000
H	1.470135000	4.792178000	1.792936000
C	-1.795509000	4.342487000	0.758664000
H	-2.164303000	4.137183000	1.768235000
H	-2.051271000	5.376494000	0.507468000
H	-2.314218000	3.672946000	0.065347000

Complex **4**

C	-2.302766000	-2.516484000	-0.018849000
C	-2.407355000	-3.924562000	-0.035435000
H	-3.381095000	-4.396272000	-0.042794000
C	-1.252010000	-4.664861000	-0.040997000
H	-1.284721000	-5.750647000	-0.052631000
C	-0.001110000	-4.007163000	-0.031263000
C	-0.000813000	-2.590939000	-0.016890000
C	1.249513000	-4.665457000	-0.034187000

H	1.281787000	-5.751264000	-0.044827000
C	2.405153000	-3.925677000	-0.022661000
H	3.378682000	-4.397864000	-0.023073000
C	2.301175000	-2.517489000	-0.010503000
C	3.557217000	-1.649069000	0.005479000
C	3.666259000	-0.786910000	-1.253438000
C	4.732903000	-0.951967000	-2.130210000
H	5.493250000	-1.697904000	-1.937064000
C	4.792634000	-0.132513000	-3.252669000
H	5.612387000	-0.235505000	-3.957263000
C	3.796783000	0.816129000	-3.458341000
H	3.811154000	1.474682000	-4.320116000
C	2.769609000	0.909037000	-2.529052000
H	1.965728000	1.632481000	-2.632228000
C	3.637280000	-0.801555000	1.276541000
C	4.669485000	-0.991755000	2.188724000
H	5.426054000	-1.746298000	2.014848000
C	4.699608000	-0.185236000	3.321839000
H	5.492072000	-0.307332000	4.054096000
C	3.709848000	0.774822000	3.502694000
H	3.702566000	1.423465000	4.372075000
C	2.717688000	0.891908000	2.538471000
H	1.919406000	1.624439000	2.620303000
C	-3.558331000	-1.647290000	-0.013318000
C	-3.646768000	-0.781861000	-1.271662000
C	-4.688297000	-0.955325000	-2.176530000
H	-5.446526000	-1.708834000	-2.005412000
C	-4.724841000	-0.134241000	-3.298943000
H	-5.524469000	-0.243269000	-4.025466000
C	-3.732002000	0.823219000	-3.476632000
H	-3.729274000	1.482740000	-4.337825000
C	-2.730530000	0.923271000	-2.520152000
H	-1.929318000	1.652790000	-2.599892000
C	-3.657101000	-0.803875000	1.259129000
C	-4.712433000	-0.987120000	2.145944000
H	-5.471228000	-1.734216000	1.951386000
C	-4.763253000	-0.184115000	3.280675000
H	-5.574209000	-0.301598000	3.993139000
C	-3.770110000	0.766890000	3.488381000
H	-3.778015000	1.413117000	4.359515000
C	-2.754074000	0.878077000	2.548907000
H	-1.952574000	1.604009000	2.653294000
N	1.149619000	-1.878786000	-0.009415000
N	-1.150961000	-1.878292000	-0.009847000
N	2.706730000	0.120442000	-1.450960000
N	2.683584000	0.115960000	1.450340000
N	-2.690288000	0.133327000	-1.442338000

N	-2.699648000	0.105165000	1.459102000
F	4.642793000	-2.503619000	0.012590000
F	-4.644626000	-2.500919000	-0.025136000
Cu	1.163456000	0.237062000	-0.020477000
Cu	-1.163264000	0.237154000	0.022360000
C	0.015145000	4.066534000	0.701133000
C	-0.015382000	4.067446000	-0.693284000
C	0.030632000	5.241657000	1.430358000
C	-0.031457000	5.243369000	-1.421166000
C	0.014637000	6.438253000	0.703157000
H	0.053895000	5.231768000	2.515747000
C	-0.016075000	6.439108000	-0.692562000
H	-0.054734000	5.234682000	-2.506571000
H	0.025928000	7.383322000	1.238209000
H	-0.027875000	7.384815000	-1.226482000
O	-0.024770000	2.782965000	-1.143774000
O	0.025076000	2.781492000	1.149990000
B	0.000240000	1.926274000	0.002663000

9. Electrochemistry

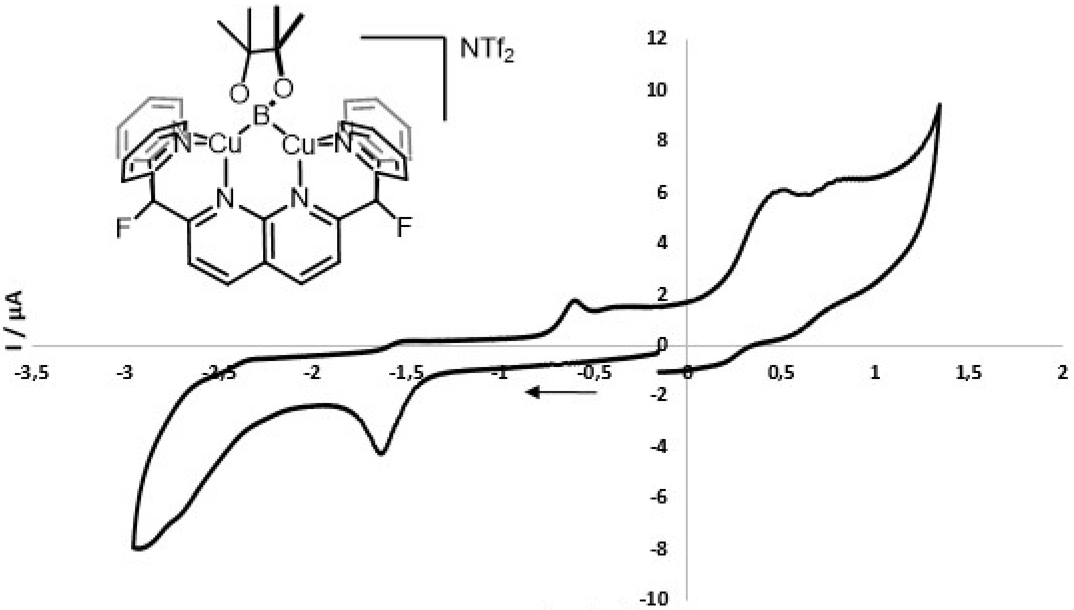

Figure S43. Cyclic voltammogram of a 0.77 mM solution of **2** in THF with 0.1 M [^{n}Bu$_4$N][PF$_6$] supporting electrolyte. The arrow indicates the initial potential and scanning direction. All redox events are observed as well when scanning in the reverse direction. This voltammogram exhibits an irreversible reduction feature ($E_{red,1}$ = -1.63 V) and three irreversible oxidation features ($E_{ox,1}$ = -0.59 V, $E_{ox,2}$ = 0.46 V and $E_{ox,3}$ = 0.78 V) before reaching the edges of the solvent window.

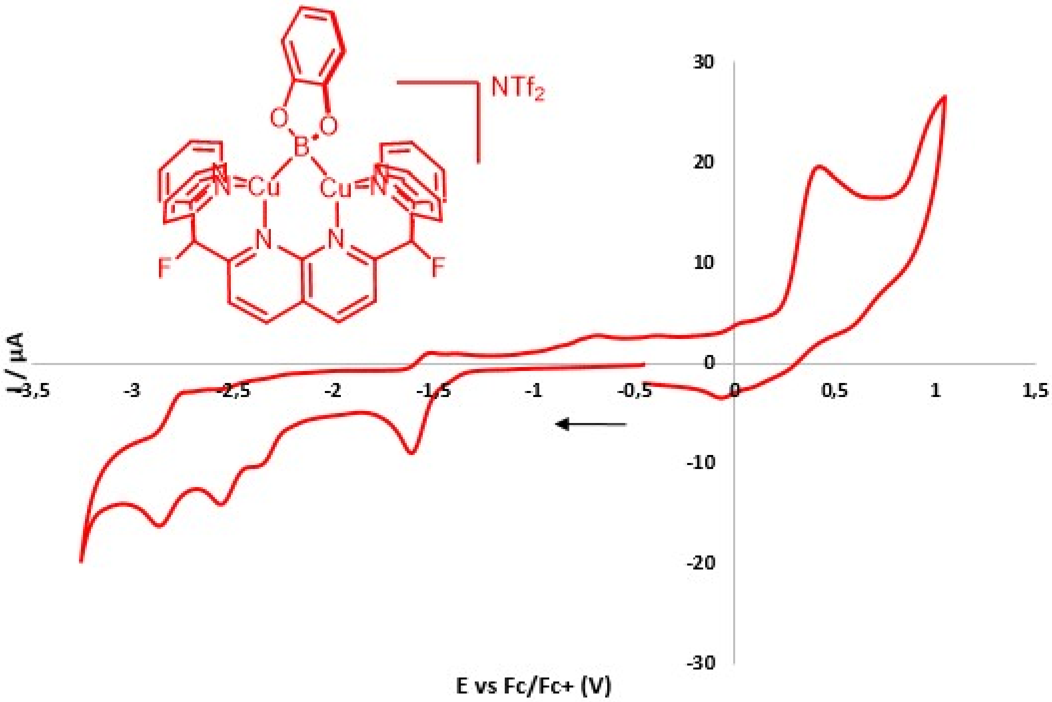

Figure S44. Cyclic voltammogram of a 0.78 mM solution of **4** in THF with 0.1 M [^{n}Bu$_4$N][PF$_6$] supporting electrolyte. The arrow indicates the initial potential and scanning direction. All redox events are observed as well when scanning in the reverse direction. This voltammogram exhibits three irreversible reduction features ($E_{red,1}$ = -1.60 V, $E_{red,2}$ = -2.36 V and $E_{red,3}$ = -2.56 V), three irreversible oxidation features ($E_{ox,1}$ = -1.55 V, $E_{ox,2}$ = -0.67 V and $E_{ox,3}$ = 0.39 V) and one quasi-reversible reduction feature ($E_{red,1}$ = -2.88 V) before reaching the edges of the solvent window.

10. X-ray Crystallography

Crystalline samples were prepared in a glovebox by decanting residual supernatant and immersing the crystals under a protective layer of Paratone N oil. All samples were frozen in a container of dry ice prior to data collection. Data were collected at the UC Berkeley CheXRay crystallographic facility on a Rigaku Pilatus 200K diffractometer using Cu Kα radiation (λ = 1.542 Å). Structures were solved by intrinsic phasing using the SHELXT[14] software package and refined using SHELXL[15] in the OLEX2 interface.[16]

Structure determination of 2. The solid-state molecular structure of **2** exhibits disorder of both triflimide anions in the asymmetric unit. Various restraints and constraints (SADI, RIGU, SIMU, EADP, EXYZ) were used to model the disordered triflimide molecules and to maintain physically reasonable anisotropic displacement parameters and geometries. In one instance, the disorder of the triflimide anion was modeled across two positions whose relative occupancies were refined using free variables. For the remaining anion, the disorder was modeled across three orientations which are partially overlapped. The occupancies of the three components were refined with free variables whose total occupancy was restrained to 1.0 with SUMP; the component with the smallest occupancy (ca. 9%) was refined isotropically.

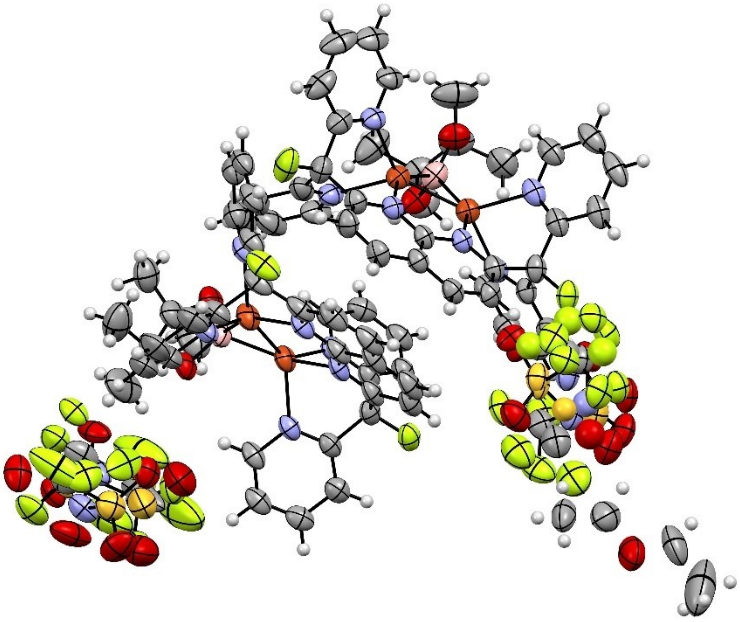

Figure S45. Solid-state molecular structure of **2**. Color scheme: C, dark gray; H, white; N, light blue; O, red; S, yellow; F, green; Cu, bronze; B, pink.

Table S3. Crystal data and structure refinement for **2**.

Empirical formula	$C_{78}H_{69}B_2Cu_4F_{16}N_{14}O_{12.5}S_4$	μ/mm $^{-1}$	2.946
Formula weight	2110.49	F(000)	4276.0
Temperature/K	100	Crystal size/mm^3	0.25 × 0.2 × 0.08
Crystal system	monoclinic	Radiation	Cu Kα (λ = 1.542 Å)
Space group	$P2_1$/n	2Θ range for data collection/°	6.876 to 149.004
a/Å	12.48590(10)	Index ranges	$-14 \leq h \leq 15$, $-40 \leq k \leq 40$, $-25 \leq l \leq 26$
b/Å	32.2974(3)	Reflections collected	122461
c/Å	21.2406(2)	Independent reflections	17501 [R_{int} = 0.0428, R_{sigma} = 0.0236]
α/°	90	Data/restraints/parameters	17501/268/1417
β/°	90.5430(10)	Goodness-of-fit on F^2	1.652
γ/°	90	Final R indexes [I>=2σ (I)]	R_1= 0.0866, wR_2= 0.25613
Volume/Å^3	8565.15(13)	Final R indexes [all data]	R_1= 0.0967, wR_2= 0.2677
Z	4	Largest diff. peak/hole / e Å^{-3}	1.67/–1.41
ρ_{calc}g/cm^3	1.637		

Structure determination of 3. The solid-state molecular structure of **3** exhibits disorder of the triflimide anion, *tert*-butoxide ligand, and co-crystallized molecule of 1,2-difluorobenzene present in the asymmetric unit. The occupancies of these disordered fragments were refined using free variables. Various restraints and constraints (SADI, SIMU, RIGU, and EADP) were used to model the disordered triflimide molecules and to maintain physically reasonable anisotropic displacement parameters and geometries. A solvent mask was used to account for a disordered, partially occupied (occu = 0.75) 1,2-

difluorobenzene molecule. A residual electron density peak was noted near atom O1A of the minor component of the disordered triflimide molecule. This peak could not be assigned in a chemically reasonable fashion, and was left as-is. There are no indications in the data to suggest twinning.

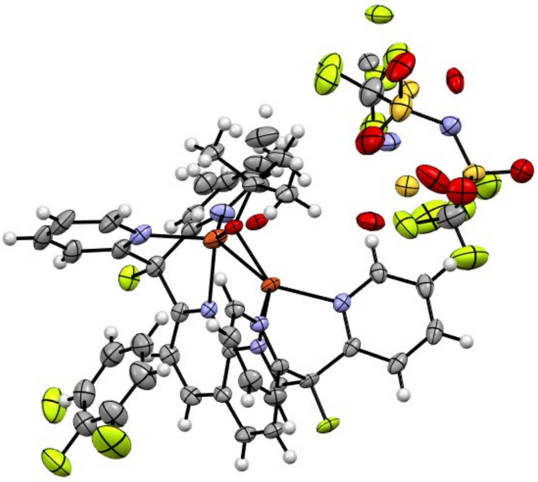

Figure S46. Solid-state molecular structure of **3**. Color scheme: C, dark gray; H, white; N, light blue; O, red; S, yellow; F, green; Cu, bronze.

Table S4. Crystal data and structure refinement for **3**.

Empirical formula	$C_{42}H_{33}Cu_2F_{10}N_7O_5S_2$	μ/mm^{-1}	2.983
Formula weight	1096.95	F(000)	1108.0
Temperature/K	100	Crystal size/mm^3	0.08 × 0.06 × 0.06
Crystal system	triclinic	Radiation	Cu Kα (λ = 1.542 Å)
Space group	*P*–1	2Θ range for data collection/°	6.89 to 149.004
a/Å	12.9678(3)	Index ranges	–16 ≤*h*≤ 16, –17 ≤*k*≤ 17, –18 ≤*l*≤ 16
b/Å	14.3694(4)	Reflections collected	45880
c/Å	14.5813(4)	Independent reflections	8865 [R_{int} = 0.0297, R_{sigma} = 0.0194]
α/°	63.797(3)	Data/restraints/parameters	8865/51/759
β/°	69.859(2)	Goodness-of-fit on F^2	1.054
γ/°	65.255(3)	Final R indexes [I>=2σ (I)]	R_1= 0.0744, wR_2= 0.1838
Volume/Å^3	2171.18(12)	Final R indexes [all data]	R_1= 0.0760, wR_2= 0.1848
Z	2	Largest diff. peak/hole / e Å^{-3}	2.96/–1.59
ρ_{calc}g/cm^3	1.678		

Structure determination of 4. The solid-state molecular structure of **4** exhibits disorder of the triflimide anion present in the asymmetric unit. The two occupancies of the triflimide anion were refined using free variables. Various restraints and constraints (SADI, RIGU, and EADP) were used to model the disordered triflimide molecules and to maintain physically reasonable anisotropic displacement parameters and geometries.

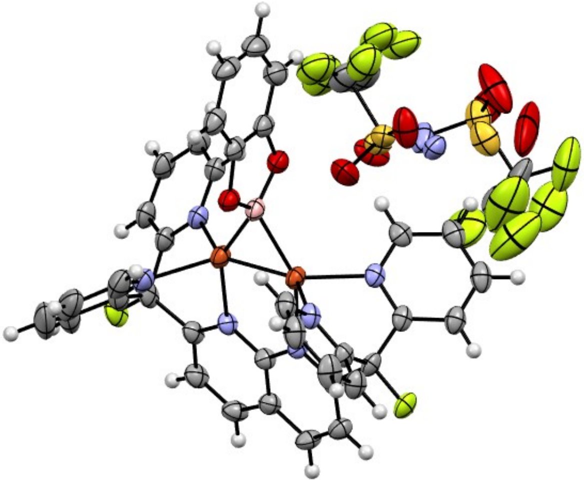

Figure S47. Solid-state molecular structure of **4**. Color scheme: C, dark gray; H, white; N, light blue; O, red; S, yellow; F, green; Cu, bronze; B, pink.

***Table S5**. Crystal data and structure refinement for **4**.*

Empirical formula	$C_{38}H_{24}BCu_2F_8N_7O_6S_2$	μ/mm^{-1}	2.837
Formula weight	1028.65	F(000)	2064.0
Temperature/K	100.15	Crystal size/mm^3	0.26 × 0.15 × 0.07
Crystal system	monoclinic	Radiation	Cu Kα (λ = 1.542 Å)
Space group	$P2_1$/n	2Θ range for data collection/°	7.182 to 149.008
a/Å	13.31060(10)	Index ranges	$-16 \le h \le 15$, $-25 \le k \le 28$, $-19 \le l \le 18$
b/Å	22.6847(3)	Reflections collected	48153
c/Å	15.3728(2)	Independent reflections	9029 [R_{int} = 0.0393, R_{sigma} = 0.0254]
α/°	90	Data/restraints/parameters	9029/75/680
β/°	107.6180(10)	Goodness-of-fit on F^2	1.103
γ/°	90	Final R indexes [I>=2σ (I)]	R_1= 0.0830, wR_2 0.1948
Volume/Å^3	4424.05(9)	Final R indexes [all data]	R_1= 0.0863, wR_2= 0.1964
Z	4	Largest diff. peak/hole / e Å^{-3}	0.90/−1.26
ρ_{calc}g/cm^3	1.544		

11. References

1) M. S. Ziegler, D. S. Levine, K. V. Lakshmi and T. D. Tilley, *J. Am. Chem. Soc.,* **2016**, *138*, 6484-6491.
2) S. Pietsch, E. C. Neeve, D. C. Apperley, R. Bertermann, F. Mo, D. Qiu, M. S. Cheung, L. Dang, J. Wang, U. Radius, Z. Lin, C. Kleeberg and T. B. Marder, *Chem. Eur. J.*, **2015**, *21*, 7082-7099.
3) T. R. Hoye, B. M. Eklov, T. D. Ryba, M. Voloshin and L. J. Yao, *Org. Lett.,* **2004**, *6*, 953-956.
4) Y. Pang, M. Leutzsch, N. Nöthling and J. Cornella, *J. Am. Chem. Soc.,* **2020**, *142*, 19743-19749.

5) K. L. Bamford, S. S. Chitnis, Z-W. Qu and D. W. Stephan, *Chem. Eur. J.*, **2018**, *24*, 16014-16018.
6) Gaussian 16, Revision A.03, M. J. Frisch, G. W. Trucks, H. B. Schlegel, G. E. Scuseria, M. A. Robb, J. R. Cheeseman, G. Scalmani, V. Barone, G. A. Petersson, H. Nakatsuji, X. Li, M. Caricato, A. V. Marenich, J. Bloino, B. G. Janesko, R. Gomperts, B. Mennucci, H. P. Hratchian, J. V. Ortiz, A. F. Izmaylov, J. L. Sonnenberg, D. Williams-Young, F. Ding, F. Lipparini, F. Egidi, J. Goings, B. Peng, A. Petrone, T. Henderson, D. Ranasinghe, V. G. Zakrzewski, J. Gao, N. Rega, G. Zheng, W. Liang, M. Hada, M. Ehara, K. Toyota, R. Fukuda, J. Hasegawa, M. Ishida, T. Nakajima, Y. Honda, O. Kitao, H. Nakai, T. Vreven, K. Throssell, J. A. Montgomery, Jr., J. E. Peralta, F. Ogliaro, M. J. Bearpark, J. J. Heyd, E. N. Brothers, K. N. Kudin, V. N. Staroverov, T. A. Keith, R. Kobayashi, J. Normand, K. Raghavachari, A. P. Rendell, J. C. Burant, S. S. Iyengar, J. Tomasi, M. Cossi, J. M. Millam, M. Klene, C. Adamo, R. Cammi, J. W. Ochterski, R. L. Martin, K. Morokuma, O. Farkas, J. B. Foresman, and D. J. Fox, Gaussian, Inc., Wallingford CT, 2016.
7) C. Adamo and V. Barone, *J. Chem. Phys.,* **1999**, *110*, 6158-6170.
8) S. Grimme, S. Ehrlich and L. Goerigk, *J. Comp. Chem.,* **2011**, *32*, 1456-1465.
9) a) W. J. Hehre, R. Ditchfield and J. A. Pople, *J. Chem. Phys.,* **1972**, *56*, 2257-2261; b) P. C. Hariharan and J. A. Pople, *Theor. Chim. Acta.,* **1973**, *28*, 213-222.
10) M. Dolg, U. Wedig, H. Stoll and H. Preuss, *J. Chem. Phys.,* **1987**, *86*, 866-872.
11) E. D. Glendening, C. R. Landis and F. Weinhold. *NBO 6.0:* Natural bond orbital analysis program. *J. Comput. Chem.,* **2013**, *34*, 1429-1437.
12) Chemcraft - graphical software for visualization of quantum chemistry computations. https://www.chemcraftprog.com
13) T. Lu and F. Chen, *J. Comput. Chem.,* **2012**, *33*, 580-592.
14) Sheldrick, G. M. *SHELXT*– Integrated Space-Group and Crystal-Structure Determination. *Acta Crystallogr.* **2015**, *A71*, 3–8.
15) Sheldrick, G. M. Crystal Structure Refinement with SHELXL. *Acta Cryst* **2015**, *C71*, 3–8.
16) Dolomanov, O. V.; Bourhis, L. J.; Gildea, R. J.; Howard, J. A. K.; Puschmann, H. OLEX2: A Complete Structure Solution, Refinement and Analysis Program. *J Appl Cryst* **2009**, *42*, 339–341.